SENSITIVITY ENHANCEMENT USING DIFFERENT DESIGN CONFIGURATIONS FOR PHOTONIC CRYSTAL WAVEGUIDE APPLICATIONS

Thesis submitted towards the partial fulfillment of requirement

for the award of degree of

Master of Engineering

In

Electronics and Communication Engineering

Submitted by:

Harshita Chopra

Roll No: 801461010

Under the guidance of:

Dr. R.S. Kaler

Senior Professor, ECED

ELECTRONICS AND COMMUNICATION ENGINEERING DEPARTMENT

THAPAR UNIVERSITY

(Established under the section 3 of UGC Act, 1956)

PATIALA – 147004 (PUNJAB)

DECLARATION

I **Harshita Chopra** hereby declare that this dissertation entitled "**Sensitivity Enhancement Using Different Design Configurations for Photonic Crystal Waveguide Applications**" in partial fulfilment for the award of degree of Masters in Engineering in Electronics and Communication Engineering from Thapar University, Patiala, Punjab is an authentic record of my own work carried under the supervision of **Dr. R.S. Kaler**.

The work has not been submitted partially or fully to any other University or Institute for the award of this or any other degree.

Date: 11/7/16

(Harshita Chopra)

Roll no. : 801461010

This is certified that the above statement made by the candidate is correct to the best of my knowledge.

Date: 11/7/16

(Dr. R.S. Kaler)

Senior Professor & Deputy Director,

ECED, Thapar University,

Patiala, Punjab, India

Countersigned by:

(Dr. Sanjay Sharma)

Professor and Head (ECED)

Thapar University, Patiala

(Dr. S.S. Bhatia)

Dean of Academic Affairs

Thapar University, Patiala

ACKNOWLEDGMENT

The real spirit of achieving a goal is through the way of excellence and austere discipline. I would have never succeeded in completing my task without the cooperation, encouragement and help provided to me by various personalities. With deep sense of gratitude I express my sincere thanks to my esteemed and worthy supervisor, **Dr. R.S. Kaler, Senior Professor and Deputy Director**, Department of Electronics and Communication Engineering, Thapar University, Patiala for his valuable guidance in carrying out work under his effective supervision, encouragement, enlightenment and cooperation. Most of the novel ideas and solutions found in this thesis are the result of our numerous stimulating discussions. His feedback and editorial comments were also invaluable for writing of this thesis.

I shall be failing in my duties if I don't express my deep sense of gratitude towards **Mr. Balveer Painam, Junior Research Fellow,** Electronics and Communication Engineering Department, Thapar University, for his inquisitiveness, insight, and inspiration. I have benefited tremendously from his countless efforts and dedication for the completion of the dissertation. I express gratitude to **Dr. Amit Kumar Kohli, Associate Professor and P.G. Coordinator**, Electronics and Communication Engineering Department, Thapar University for inspired motivation to give the best of the potential at each step.

I would like to thank all friends who supported me throughout the course of this work. I would like to pay my gratitude towards my parents, who have always supported me in doing the things my way and whose everlasting desires, encouragement, affectionate blessings and help made it possible for me to complete my degree. I would also like to render my gratitude to the Almighty God who bestowed self-confidence, ability and strength in time to complete this task and for not letting me down at the time of crisis and showing me the silver lining in the dark clouds.At last but not the least I would like to thank all those who have provided their help in a direct or indirect manner to achieve this goal.

Harshita Chopra

801461010

ABSTRACT

In this work, three types of sensors have been designed. In the first type, a ring shaped photonic crystal waveguide is designed using finite difference time domain method. This waveguide can be used for gas sensing applications. After introducing the line defect, transmission spectra was obtained with different hole diameters. With the increase in hole diameter, the sensitivity increases. Further enhancement in sensitivity was measured by etching in silicon guiding layer and up to a certain depth in the buried oxide layer. It was observed that the sensitivity increases up to certain etch depth after which it is found to be decreasing. After this, infiltration with different gaseous analytes was done to measure the sensitivity based on the shift in the cut off wavelength as observed because of the change in refractive index of the structure. The experimental results showed that the ring shaped structure had a sensitivity value of 675nm/RIU. This sensor can be used to sense different gases like hydrogen, ammonia, nitrogen etc.

In the second type, a 2-D photonic crystal waveguide based biosensor is designed with a diamond shaped ring resonator and two waveguides-a bus waveguide and a drop waveguide. The sensing mechanism is based on change in refractive index of the analytes as explained above leading to a shift in the peak resonant wavelength. This mechanism can be used in the field of bio-medical treatment where different body fluids such as blood, tears, saliva or urine can be used as the analyte in which different components of the fluid can be detected. It can also be used to differentiate between the cell lines of a normal and an unhealthy human being. Average value of quality factor for this device comes out to be 1082.2063. Sensitivity values increases with the increase in RI. For 0.02 change in RI, sensitivity increases by 0.0154nm/RIU.

Finally we design three dimensional (3-D) photonic crystal waveguides using group III-V semiconductor materials and study the effect of different directions of light propagation for each of these materials. The presence of photonic band gaps (PBG's) in photonic crystals can be used to control the direction of propagation of light by

prohibiting light flow at a certain frequency range in certain directions. Semiconductor materials posses a forbidden energy gap between valence band and conduction band of electrons. Thus, an analogy can be drawn between the behaviour of electrons in case of semiconductors and that of light in case of photonic crystals. Silicon based waveguide is first designed and then integrated with different group III-V semiconductors. The sensitivity values are calculated and compared for each of these materials with respect to silicon based waveguides. The designed structure consists of holes filled with water in a silicon/silicon and semiconductor configuration and the refractive index is varied from 1.33 to 1.45. Corresponding shift in peak wavelength is measured and the sensitivity values are calculated for the same. Among all the materials, Indium phospide seems to be the most appropriate choice based on the light transmission with an average sensitivity of 201.76 nm/RIU obtained by infiltration of holes with various analytes.

LIST OF PUBLICATIONS

1. H. Chopra, R.S. Kaler, and B. Painam, "Sensitivity enhancement of photonic crystal waveguide based sensor using ring shaped holes," Journal of Nanoelectronics and Optoelectronics (Accepted: 16/04/2016).

CONTENTS

LIST OF FIGURES

LIST OF TABLES

LIST OF ACRONYMS

1. One dimensional-**1D**
2. Two dimensional-**2D**
3. Three dimensional -**3D**
4. Photonic crystal-**PC**
5. Transverse Electric- **TE**
6. Transverse Magnetic-**TM**
7. Photonic Band Gap- **PBG**
8. Silicon-on-Insulator-**SOI**
9. Photonic Crystal Fibres-**PCF**
10. Photonic Crystal Waveguides-**PCW**
11. Micro-Electro-Mechanical system- **MEMS**
12. Refractive Index –**RI**
13. Group Velocity Dispersion-**GVD**
14. Refractive Index Unit-**RIU**
15. Finite Difference Time Domain-**FDTD**
16. Silicon dioxide-**SiO2**
17. Aluminium Arsenide-**AlAs**
18. Gallium Aluminium Arsenide-**GaAlAs**
19. Plane Wave Expansion-**PWE**
20. Ring shaped photonic crystals-**RPhC's**
21. Very Large Scale Integration –**VLSI**
22. Complementary Metal Oxide Semiconductor-**CMOS**
23. Aluminium Nitride-**AlN**
24. Indium Phospide-**InP**
25. Indium Nitride-**InN**
26. Electron Volt-**eV**
27. Magnetic Resonance Imaging-**MRI**
28. World Health Organization-**WHO**
29. Red Blood Cell-**RBC**
30. White Blood Cell-**WBC**
31. Deoxyribonucleic Acid-**DNA**

32. Quality Factor-**Q**

33. Full Width Half Maximum-**FWHM**

CHAPTER 1

INTRODUCTION

1.1 OVERVIEW ON PHOTONIC CRYSTAL WAVEGUIDE

A new revolution has been introduced in the field of optical communications with the new technologies which are based on waveguides and optical fibres. Hence, efforts have been made in the past decades to control the light propagation in various directions, to forbid light from passing in certain directions or to confine it in some other directions. In devices such as dielectric mirrors, Bragg diffraction was used as a way of controlling light. Thus a new class of materials known as photonic crystals (PC) was invented based on the light reflection that was produced by the principle used in dielectric materials. These are regularly shaped materials with periodic dielectric constant. If we consider that the input light which is incident on the crystal has a wavelength with the same magnitude order as that of periodicity, waves that are scattered at the interfaces interfere with each other, giving rise to a band structure. A photonic band gap (PBG) refers to range of frequencies that are forbidden through the crystal occurs when there is a high difference between the dielectric constants of the materials which make up the photonic crystal. For three dimensional (3D) crystals, a perfect band gap is obtained. Two dimensional (2D) crystals offer the same properties as their 3D equivalent and are easier to fabricate. 2D crystals have homogeneity in the third dimension but scattering losses may occur in this direction. These photonic crystals show interesting effects such as modification of spontaneous emission, birefringence effect, super-prism effect, negative refraction, and the existence of band gap for waveguides [1] which can be used in various applications. The periodicity of the photonic crystal is broken by introducing defects, hence making it possible to introduce light in required direction [2]. Devices such as Mach-Zehnder interferometer, directional coupler [3], resonator [4], waveguide [5], etc, are realized with the use of structures based on photonic crystals.

1.2 STRUCTURAL AND THEORETICAL MODEL OF PHOTONIC CRYSTAL

PC can be divided into 1-D, 2-D and 3-D structures, as shown in Fig 1 based on refractive index distribution. Structures where we see periodicity only in a single dimension are known as 1D photonic crystal. By this we mean that the refractive index is periodic in that dimension while in the other two dimensions it is homogenous in nature. In case of a planar waveguide, if we add transversal elements along the direction of propagation, there is a periodic modulation of refractive index. Hence a 1D structure can be obtained in planar waveguides.

In case of 2D structures, we can see a periodic variation of refractive index in two dimensions while in the third dimension, there is no such variation. Common types of 2D structures include holes etched in a material of higher refractive index.

3D structures however have periodic variation of refractive index in all the three dimensions. 2D photonic crystals offer same properties as 3D crystals and can be easily fabricated. Hence, they are used widely for generating slow light. Generally, 2D photonic crystal slabs are of two types: one showing transverse magnetic (TM) band gap which are based on dielectric rods in air configuration; and the other showing transverse electric (TE) band gap based on air holes in dielectric background. In TE-like polarization electric field is parallel to surface of wafer and in TM-like polarization electric field is perpendicular to surface of wafer. Fig 2 shows the PBG of a 2D slab: x-axis shows the direction of electromagnetic wave which is incident on the crystal, z-axis shows the normalized light frequency, and the middle part (shaded light block) shows the required band gap. The light waves with frequencies lying within this band gap region cannot pass through PC. So, due to absence of the corresponding mode, they will be reflected back completely whenever electromagnetic waves are incident on the crystal.

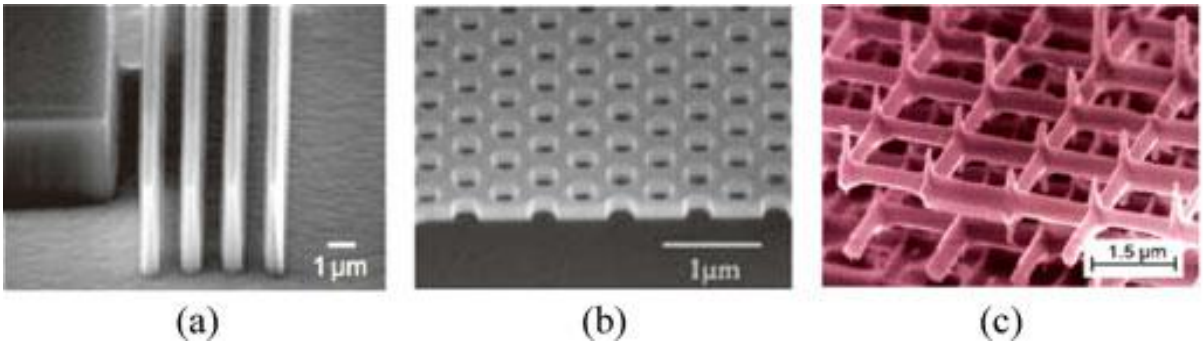

Fig1 (a) 1-D, (b) 2-D (c) 3-D photonic crystal waveguides [2]

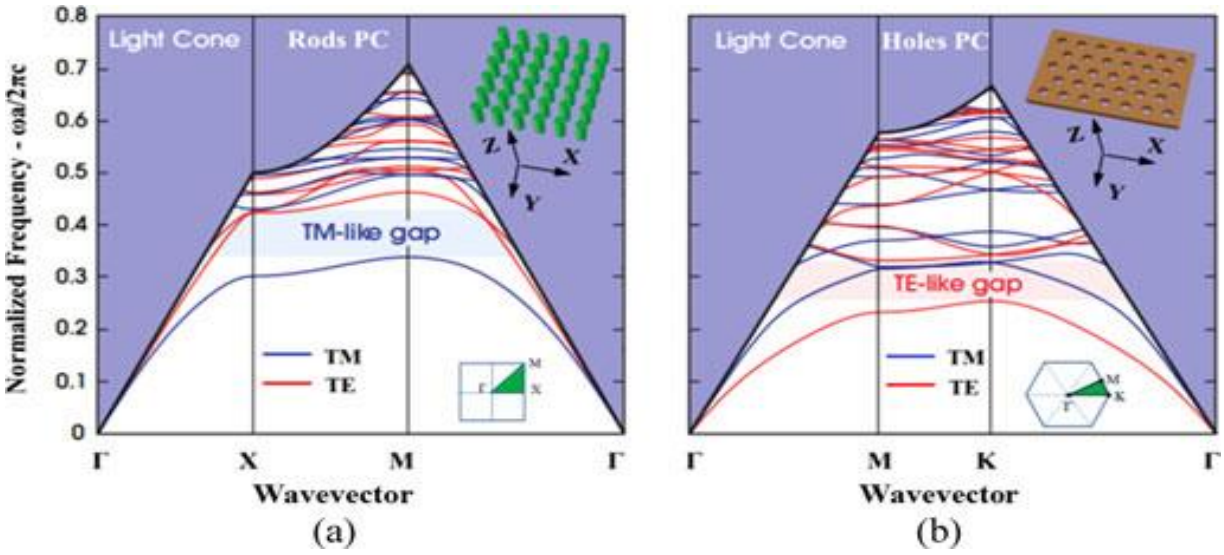

Fig2 Band diagrams for 2-D Photonic crystal: (a) the rods photonic crystal (b) holes photonic crystal [2].

1.3 WAVE PROPAGATION IN A HOMOGENOUS MEDIUM

Before we consider the propagation of wave in a photonic crystal, let us consider a dielectric medium which is linear, homogenous and isotropic i.e. in a free space. Equation (1)-(4) shown describe Maxwell's equation in a differential form [1]:

$$\nabla \times E = -\frac{\partial B}{\partial t} \tag{1}$$

$$\nabla \times H = \frac{\partial D}{\partial t} + J \tag{2}$$

$$\nabla . D = \rho \tag{3}$$

$$\nabla . B = 0 \tag{4}$$

Here, E is the electric field in volts/meter, H is the magnetic field in ampere/meter, D is the electric field displacement in coulomb/meter^2, B is the magnetic induction field measured in Tesla, ρ is the free charge density measured in coulomb/meter^3 and J is the free current density in ampere/meter^2.

D and B can be written in the form of relative permeability μ_r and dielectric constant ε_r as:

$$D = \varepsilon_o \varepsilon_r E = \varepsilon E \tag{5}$$

$$B = \mu_o \mu_r H = \mu H \tag{6}$$

In a free space, μ_r and ε_r depend on the frequency. But if we consider that the system is free of sources and there is no dispersion, the Maxwell's equations take the form:

$$\nabla^2 E(r,t) - \mu\varepsilon \frac{\partial^2 E(r,t)}{\partial t^2} = 0 \tag{7}$$

$$\nabla^2 B(r,t) - \mu\varepsilon \frac{\partial^2 B(r,t)}{\partial t^2} = 0 \tag{8}$$

On solving these two equations, we get plane waves travelling at a speed *v*.

$$v = \frac{1}{\sqrt{\varepsilon\mu}} = \frac{c}{\sqrt{\mu_r \varepsilon_r}} = \frac{c}{n} \tag{9}$$

Where c is the speed of light in vacuum, r represents the displacement, t represents time and n is the refractive index. Using this, we rewrite equation (7) and (8):

$$\left(\frac{c}{n}\right)^2 \nabla^2 E(r,t) - \frac{\partial^2 E(r,t)}{\partial t^2} = 0 \tag{10}$$

$$\left(\frac{c}{n}\right)^2 \nabla^2 B(r,t) - \frac{\partial^2 B(r,t)}{\partial t^2} = 0 \tag{11}$$

Electric field can be written as a superposition of different waves as given by equation (12), where E_0 is the amplitude, ω is the angular frequency and k represents the direction of propagation of wave.

$$E(r,t) = \mathrm{Re}(E_o e^{jkr} e^{-jwt}) \tag{12}$$

Next, the relation between ω and k is given as the dispersion relation and the relation shows that the frequency of the wave depends on the refractive index n of the medium as given below:

$$v_p = \frac{\omega}{k} = \frac{c}{n} \tag{13}$$

If our material is homogenous the group velocity and phase velocity are the same. But when the material is non homogenous, considering that the input wave is associated with a bandwidth, the phase velocity v_p is given as in equation (13) and the group velocity is the derivate of the above equation. So v_g is given as:

$$v_g = \frac{\partial w}{\partial k} = 2\pi \frac{\partial f}{\partial k} \tag{14}$$

1.3.1 1D STRUCTURES

As discussed above, 1D structure are periodic in a single dimension only. Fig 3 below represents a structure having alternating layers of materials having refractive indices n1 and n2. The structure repeats itself after a period 'a' which represents the lattice constant. Hence the refractive index becomes periodic with a relation $n(z) = z+Za$, where z is the direction in which refractive index is periodic while it is homogenous in the x and y directions, Z is an integral multiple of lattice constant 'a'.

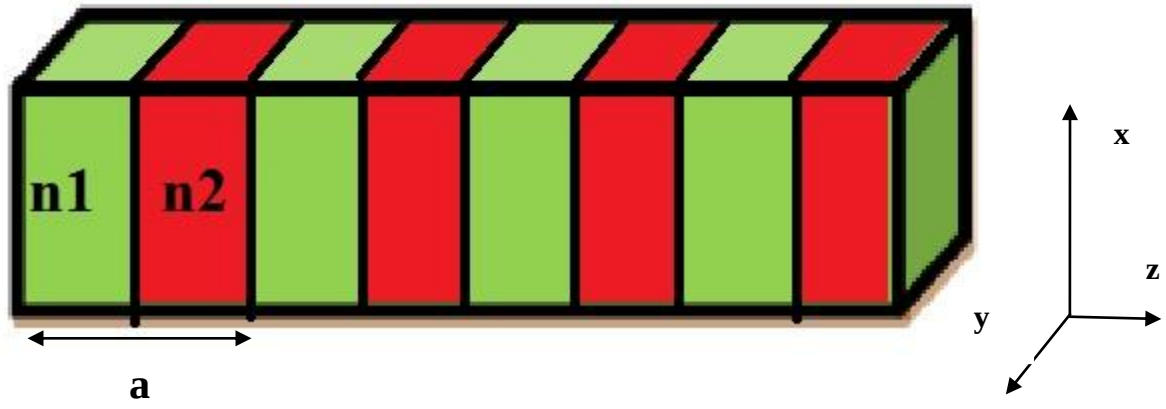

Fig 3 1D structure with alternating layers of materials having refractive indices n1 and n2.

Such variation in periodicity leads to periodicity of the wave travelling through the medium. According to Bloch theorem, this wave is modulated by a function $u_k(z)$ which has a period equal to that of the refractive index distribution in the medium. Hence, equation (12) can be written as:

$$E(z,t) = \mathrm{Re}(u_k(z)E_o e^{jk_z(\omega)z}e^{-j\omega t}) \qquad (15)$$

Hence in the direction where the structure is periodic, these waves maintain their form and are only modified by the phase factor.

$$u_k(z) = p_k(z)e^{-jk_z z} \qquad (16)$$

The above equation shows that the wave only gets modulated by the phase factor. Due to the periodicity in the structure, each wave vector can now be associated with infinite number of solutions having different frequencies instead on one as explained above. These solutions show that the frequencies can be expressed as a function of k. These solutions are known as band diagram. $p_k(z)$, here is a periodic function which depends on the lattice constant 'a'.

Suppose we have two values of propagation constant k_z and $k_{z'}$ which have the same value of phase factor such that $k_{z'} = k_z + h.\frac{2\pi}{a}$. In the direction of our lattice, the solution can be obtained if we consider the values of k in the interval $\frac{2\pi}{a}$ assuming all the modes together. Thus the region between $-\frac{\pi}{a}$ and $\frac{\pi}{a}$ is known as Brillouin zone.

1.3.2 2D STRUCTURES

As explained earlier, 2D crystals have periodic variation of refractive index in two dimensions as compared to a single dimension in 1D crystal. Consider periodicity in x and z directions and homogeneity in y direction as shown in Fig 4.

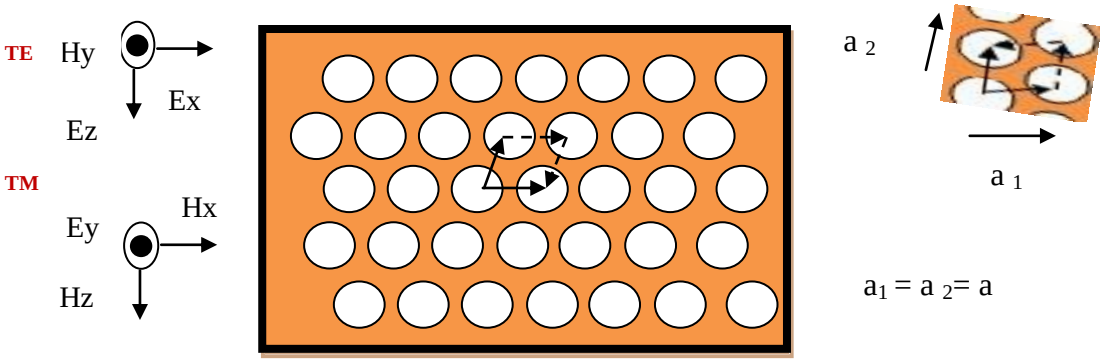

Fig 4 2D crystal with holes etched in a high dielectric material.

We have two values of propagation constant k_z and $k_{z'}$ such that $k_{z'} = k_z + M$. For the case of 2D crystals, M should be a linear combination of a_1 and a_2. Fig 5 shows a hexagonal shaped region known as the first Brilliouin zone such that the above two modes considered are constricted within this hexagonal shaped region only. The yellow region marked here shows the frequencies that are allowed to pass through the crystal. Hence this region is used to mark the presence of a PBG.

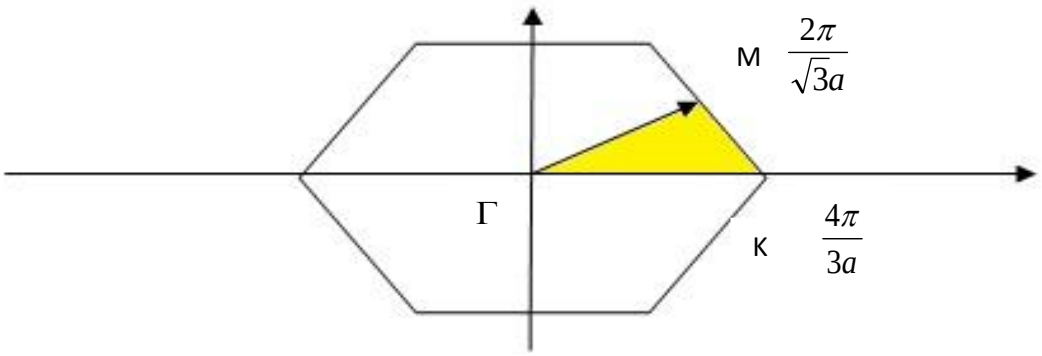

Fig 5 Hexagonal shaped region in which the yellow region marks the first brillouin zone.

It has already been explained in section 1.2 above that TE mode is used to represent air holes in a high refractive index medium whereas TM mode represents dielectric rods in a low refractive index medium. The associated band diagrams for both these polarizations have been shown in Fig 2.

1.4 HEXAGONAL GOEMETRY AND ITS COMPARISON WITH SQUARE GOEMETRY

The most commonly used photonic crystal structure consists of a triangular lattice of air holes with lattice constant ‘a’ and radius of air holes ‘r’ on a silicon-on-insulator (SOI) substrate as shown in Fig 6. The reason for choosing this geometry is as follows: As compared to the square lattice, the PBG obtained is larger than the one obtained in case of a square lattice. The symmetry of first Brillion zone for a triangular lattice is almost similar to that of air holes and is comparatively more

circular. This gap is less sensitive to variations in geometrical parameters and can be easily fabricated. To reduce the leakage of light in the vertical direction from the substrate, the material underneath the PCW can be easily removed forming a free standing membrane which is not possible in case of dielectric rods in air configuration. The light confinement within the slab is stronger due to $n_{clad} < n_{eff} < n_{core}$, where n_{eff} represents the effective refractive index of the slab, n_{core} and n_{clad} being the refractive index of the core and cladding respectively. This structure has air both below and above the slab giving rise to symmetric structure in the z-direction which is perpendicular to the plane of slab. Hence, this configuration proves best for implementation of various types of waveguides. The relationship between lattice constant 'a' and wavelength 'λ' is given as a = U • λ, where U is the normalized frequency [2]. If the structural parameters are changed proportionally, the properties of the crystal remain unchanged. Without starting a new simulation, one can choose the input wavelength before fabrication, by adjusting the lattice constant 'a'.

1.5 BASIC PROPERTIES OF PCW

If we remove the central row of air holes from the Γ-K direction, a W_1 photonic crystal waveguide is formed [2]. Further, if we shift the two PC regions closer to each other or farther away from each other, the waveguide width obtained is *i* times of that in case of W1 PCW therefore resulting in W_i PCW's. As mentioned above, when we introduce a line defect in PC, light propagates through the waveguide. The PBG obtained confines a series of guided modes in the horizontal direction. In the vertical direction, the process of total internal reflection leads to confinement of light due to difference between refractive indices of different layers. Fig 7 shows that the TE-like polarized light can be confined strongly both in horizontal and vertical directions, and the leakage of light is very small. Fig 8 shows the transmission spectra of W1 PCW without any defects. We can see that the transmission band obtained for PCW matches perfectly with the PBG obtained for PC. The light with wavelength outside that of PBG cannot pass through the waveguide. However, light with wavelengths falling inside PBG suffer from interference and reflection.

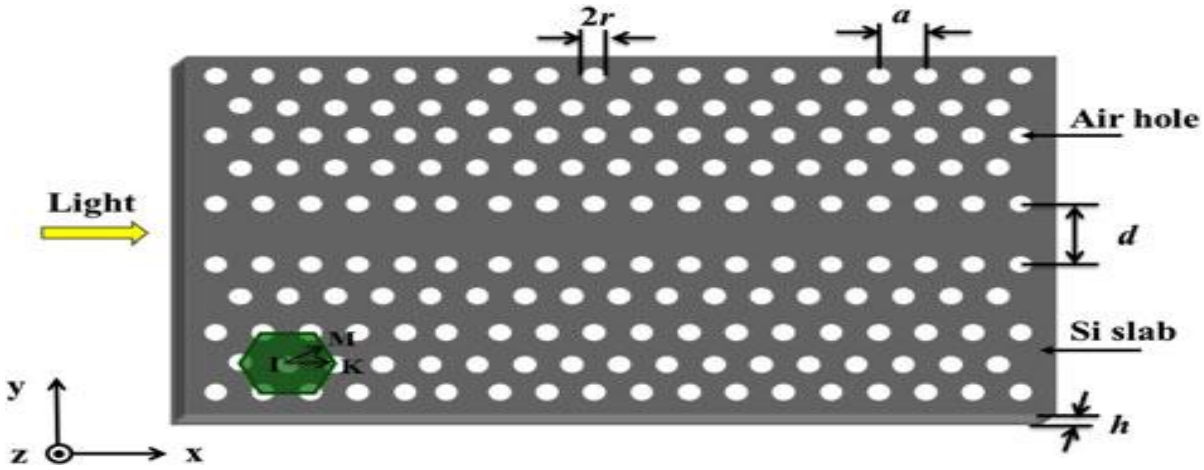

Fig 6 Basic structure ofa photonic crystal waveguide, where r is the radii of air holes, a is the lattice constant, d is the waveguide width, and h is the thickness of slab [2].

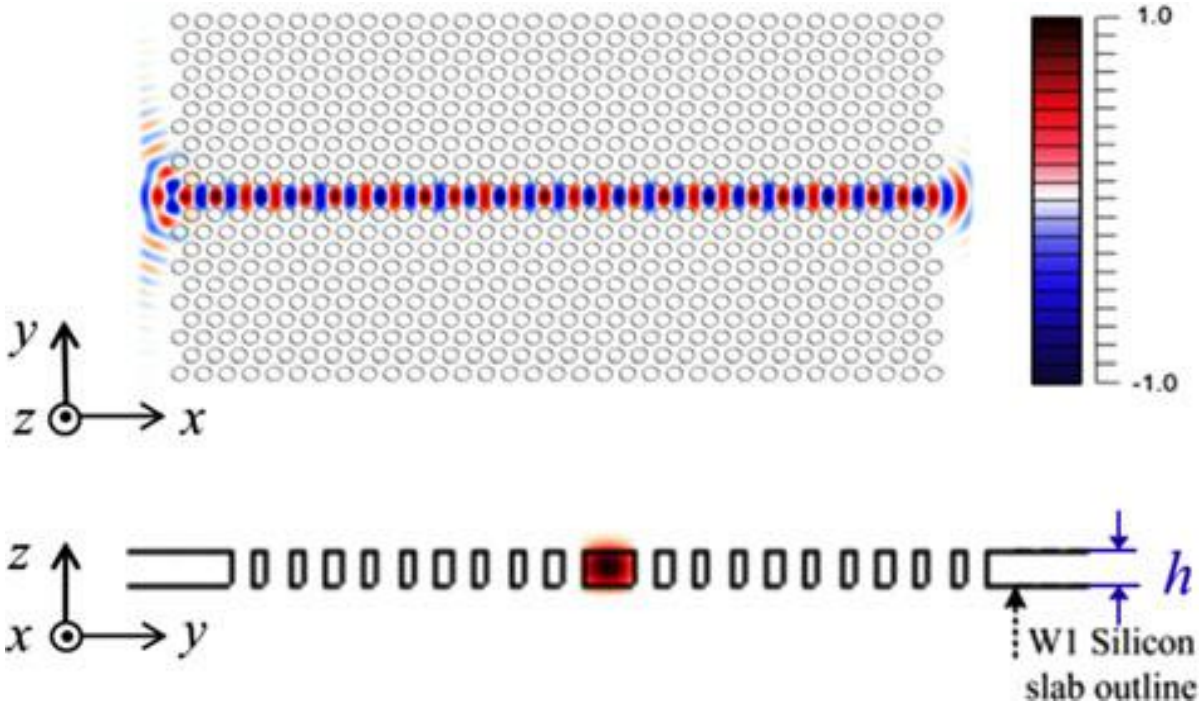

Fig 7 Electric field distribution through W_1 photonic crystal waveguide [2].

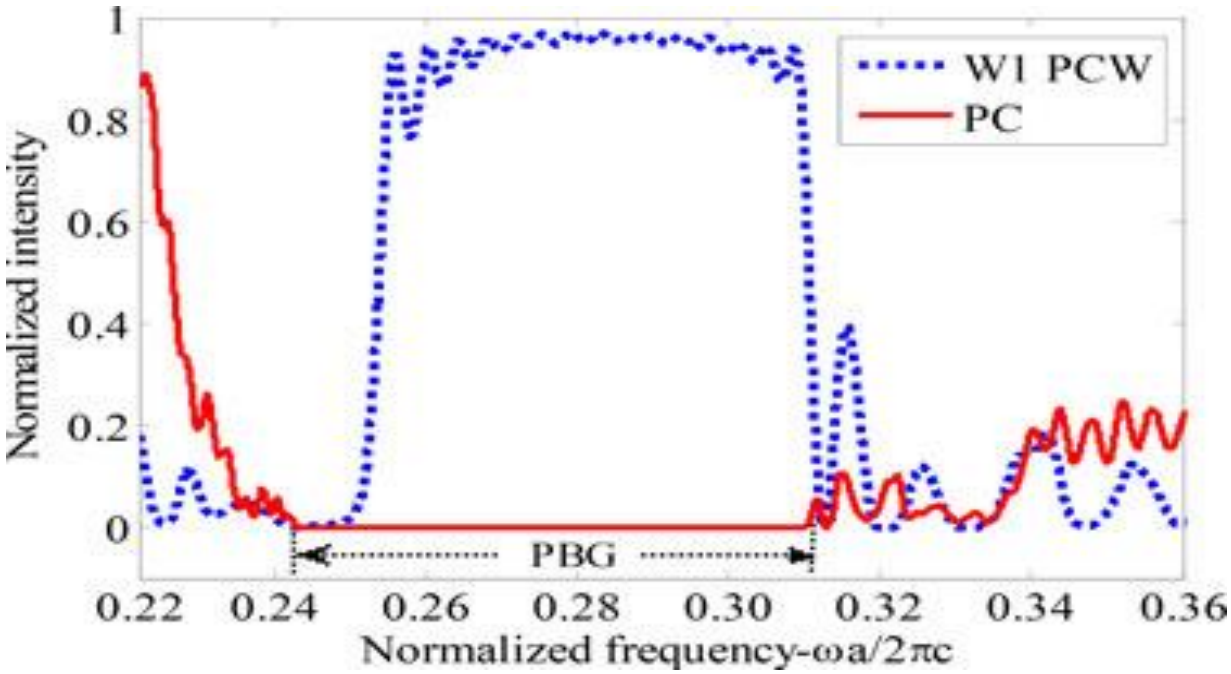

Fig 8 Transmission spectra of W_1 PCW and perfect PC without any defect [2].

Fig 9(a) shows the simplest PCW structure formed by placing circular air holes in a hexagonal geometry on top of a silicon layer in SOI substrate. The PBG is determined by the lattice constant and filling factor of the crystal. These are used in the field of refractive index based sensing applications.

PCW is then formed by introducing a line defect in this structure created by removing a row of holes leading to the trapping of light inside the waveguide effectively as shown in Fig 9(b). This structure is utilized to realize photonic devices such as coupled cavity, filter, resonator, directional coupler, splitter, etc., have been realised by utilising this structure [4].

Photonic crystals which are realized by circular holes are termed as conventional PC's. They depend on electric field polarization, thereby a full band gap is difficult to achieve. Recently, a lot of research is going on to design photonic crystals which are polarisation-independent. Hence, a full band gap structure can be obtained which does not depend on electric field polarization. Utilizing the above concept, various highly sensitive photonic crystal based platforms have been designed which can be used to sense various analytes [3].

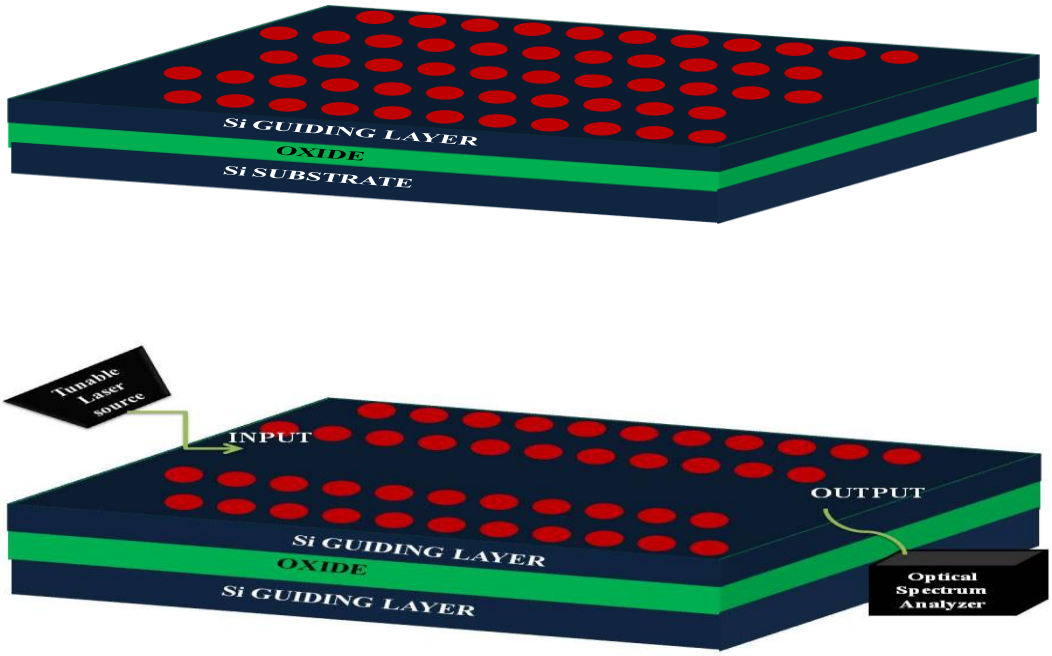

Fig 9 (a) Photonic crystal schematic with air holes on a Si background (b) Line defect obtained by removing a single row of holes.

1.6 APPLICATION AS SENSORS

PCs are known to have features such as strong field confinement, small mode volumes and low extinction losses. These features can be utilized in designing low loss inter-connects, low threshold voltage lasers and highly sensitive sensors. Due to their integration with micro-electro-mechanical system (MEMS), their application as sensors is coming out to be a promising platform. In particular, PCs are very interesting for opto-fluidic sensing applications in which fluid can be injected providing high refractive index modulation [6]. The application of a refractive index (RI) sensor has gained a high degree of interest within the last decade since it can be

applied to measure very small changes in temperature, pressure, humidity, chemical composition, etc.

Ultra compact and high sensitive micro sensors are gaining a lot of interest providing a variety of functions such as stress sensors, micro displacement sensor and biochemical sensor [7]. PC structures can be fabricated on scale of tens to hundreds of nanometres with the development of nanotechnology based crystals. It is observed in that ring shaped PCW's provide higher sensitivity values compared to those designed using circular holes [8] [9] .These sensors can be utilized to detect low concentrations of various analytes and smaller molecules with higher signal-to-noise ratio.

1.7 FACTORS CONSIDERED IN DESIGNING A PCW

- ***Materials:*** In order to obtain a wide PBG in a photonic crystal, there should be high refractive index contrast among the existing materials. Common materials used for fabrication part includes SiO_2, AlAs, GaAlAs etc. However, as explained above SOI substrate is the most common platform.

- ***Structure:*** The two configurations as discussed above include- holes in a high refractive index background and dielectric rods in a lower refractive index medium. The rod in air configuration is more complex to fabricate as compared to the other configuration because of a higher aspect ratio. This also leads to a weaker guiding of light and is associated with higher losses. Therefore, holes in a higher refractive index medium are generally preferred for simulation purposes as it is much easier to fabricate.

- ***Thickness:*** The core layer should be thin enough so that there is greater interaction between the input field and the target molecules. In such a case, sensitivity increases. However, care should be taken so that radiation losses do not increase.

- ***Wavelength range:*** This factor determines the range of operation of the device. Either 1310nm or 1550nm is taken as the central wavelength, but in most of the cases 1550nm is considered because there is a limitation of water absorption at 1310nm.

- ***Defects:*** Introducing defects in a photonic crystal leads to the formation of a photonic crystal waveguide in order to allow light to pass through the crystal for sensing purposes. These defects can be in the form of cavities, slotted waveguides, etc.

1.8 PLANE WAVE EXPANSION METHOD

By using Floquet-mode analysis, this method uses the solution of Maxwell's equations as sum of different wavelengths. Hence we can calculate the band structure or determine the presence or absence of a PBG using this method. Less number of calculations are involved in this method.

1.9 FINITE DIFFERENCE TIME DOMAIN (FDTD) METHOD

In the entire work, the simulation part is based on the finite difference time domain method. This algorithm can be used to find electromagnetic field in each direction. However, it requires a large amount of memory to run the simulations. Any minor changes that are applied to the structure can be determined using this method. The combination of features such as high degree of light confinement along with large refractive index difference among the different layers in semiconductor based devices makes it an efficient tool for simulation purposes. It is obtained by solving time-dependent Maxwell's curl equations as given below in equation (17) to (20).

$$\nabla \times E + \frac{\partial B}{\partial t} = 0 \tag{17}$$

$$\nabla \times H - \frac{\partial D}{\partial t} = J \tag{18}$$

$$\nabla.B = 0 \tag{19}$$

$$\nabla.D = \rho \tag{20}$$

Here, E is the electric field in volts/meter, H is the magnetic field in ampere/meter, D is the electric field displacement, B is the magnetic induction field, ρ is the free charge density and J is the free current density.

Considering the medium to be non-magnetic and source free, putting $J = 0$ and $\rho = 0$ and substituting $B = \mu H$ and $D = \varepsilon E$ we get Maxwell's equations in the form as given in equations (21) to (24).

$$\nabla \times E = -\frac{\partial B}{\partial t} = -\mu_o \frac{\partial H}{\partial t} \tag{21}$$

$$\nabla \times H = \frac{\partial D}{\partial t} = \varepsilon \frac{\partial E}{\partial t} \tag{22}$$

$$\nabla.B = 0 \tag{23}$$

$$\nabla.D = 0 \tag{24}$$

By expanding the E and H field into their harmonic forms, substituting in the above equations, eliminating E and rearranging the equations in terms of H, we get the Master equation as

$$\nabla \times \left[\frac{1}{\varepsilon} \nabla \times H \right] = \frac{\omega^2}{c^2} H \tag{25}$$

Equation (25) shows that an inverse relation exists between the frequency 'ω' of the propagating light and the dielectric constant 'ε' of the material.

1.10 METHODOLOGY

Photonic crystal waveguide configurations to be used for various sensing applications have been designed using Opti-FDTD software. A brief introduction about this softwares is presented below:

- **Opti-FDTD:** It allows for the design and simulation of passive and non-linear photonic components. These components are used for the propagation of wave in non-linear environments. It is a user friendly and a highly powerful software tool that uses Uniaxial Perfectly Matched Layer boundary condition. The Maxwell's equations as described above are first differentiated and solved for temporal and spatial electric and magnetic fields. Arbitrary model geometries can be designed and one can specify any number of material properties as per the requirement.

1.11 OBJECTIVES

The main objectives that have been covered in this dissertation for designing refractive index based sensors based on photonic crystal waveguides are discussed below:

• To enhance the sensitivity by engineering the structural design of photonic crystal waveguide

• In order to improve the quality factor values, amplification techniques have been adopted

• To effectively identify the most suitable semiconductor based configuration of a photonic crystal waveguide in order to decide which semiconductor material gives the best results when used for sensing applications.

1.12 OUTLINE OF THE THESIS

The thesis has been organized into the following chapters. Contents of each chapter are briefly described as under:

Chapter 1 gives the introduction about photonic crystal waveguides and its basic properties.

Chapter 2 gives the brief literature review about the previous work done in this field. Various papers based on gas based sensors, bio-sensors, sensors designed using various semiconductor materials have been discussed.

Chapter 3 of the thesis focuses on a gas based sensor that has been designed using ring shaped holes. The results have been calculated for various hole diameters and for various etch depths. Optimization for this design is done by etching the holes in the substrate layer and measuring the transmission characteristics.

Chapter 4 deals with a bio-sensor which can be used for the detection of various diseases. The design can be used for the detection of diseases related to the blood, for detection of diabetes, and for detection of various types of cancers.

Chapter 5 is based on the integration of silicon with various group 111-V semiconductor materials in order to find out the best material which can be used in designing highly sensitive sensors.

The principle used in these three chapters is based on shift in cut off wavelength as obtained by a change in RI of the analyte used, leading to a change in the sensitivity.

Chapter 6 concludes the entire work and discusses about the future work that can be done using the proposed designs.

CHAPTER 2

LITERATURE REVIEW

2.1 INTRODUCTION

The main reason why optical sensors are gaining huge interest is because they eliminate the need of radioactive labelling of molecules [6] and are highly sensitive to change in chemical composition, temperature, pressure. They save time and are effective in terms of cost. Label-free sensing techniques include optical fibres, waveguides, resonators, Plasmon resonance [6]. However, they are not really practical in terms of on-chip integration. Photonic circuits however can be easily fabricated with on-chip circuits and have small sizes.

In this thesis, we present three different types of sensor designs which can be used for detection of various gases, bio-markers for detecting diseases and in the final design we integrate silicon with various semiconductor elements to find out which semiconductor gives the best results in sensitivity and quality factor measurements. Given below is a brief discussion about the work done by various researchers in these fields.

C. Jamois et al. [1] discussed on the properties of silicon based two-dimensional photonic crystal, crystals designed using from macroporous silicon called infinite 2-D photonic crystals and slabs based on silicon-on-insulator basis. Their bulk properties including the light cone and its impact on the band structure is discussed. Their main application includes wave guiding which is discussed for both the material systems and compared with classical waveguides which are based on index grating. For modes above the light line losses are calculated.

Y. Zhao et al. [2] discussed on various optimization methods to overcome the drawbacks related to slow light. Slow light in a perfect PCW has high group index and large group velocity dispersion. Group velocity dispersion (GVD) limits the bandwidth of slow light and disturbs all the practical applications. These methods

have the ability to modify the properties of slow light by a change in their structural parameters or using external agents to change the effective refractive index. The group index, bandwidth, GVD, and normalized delay- bandwidth product is calculated for each method including their advantages and fabrication complexity.

A.K. Goyal et al. [3] proposed a ring shaped structure of holes in photonic crystal waveguides which can be used for gas sensing applications. A 3D structure is analyzed using finite difference time domain method. The ring shaped holes are etched in the silicon layer by introducing a new row of holes in the line defect. Further to increase the sensitivity, these holes are over etched up to a finite depth in the silicon oxide layer underneath the silicon layer. By varying the radius of the holes in the line defect and the etch depth the transmission characteristics and the sensitivity is measured by calculating the corresponding shift in cut-off wavelength.

A.K. Goyal et al. [4] proposed a photonic crystal waveguide based sensor in silicon-on-insulator (SOI) material with circular holes which are etched up to a finite depth in the buries oxide layer underneath the silicon guiding layer. A 3D structure is analyzed using finite difference time domain method. By varying the radius of the holes in the line defect and the etch depth the transmission characteristics and the sensitivity is measured by calculating the corresponding shift in cut-off wavelength. The average value of sensitivity obtained for refractive index values between 1.0 and 1.5 RIU is 386 nm/RIU.

H.S. Dutta et al. [5] proposed a photonic crystal waveguide based on silicon-on-insulator with ring shaped holes to realize a highly sensitive refractive index based sensor. The structure is analyzed using 3D finite difference time domain method. The structure is modified by introducing a row of holes which form the line defect. The sensitivity is further improved by replacing this row of holes by a row of ring shaped holes. A wavelength shift of 210nm is obtained for refractive index values between 1 and 1.5 RIU giving a sensitivity of 420nm/RIU.

F. Bagci et al. [6] presented a liquid based refractive index sensor. Here sensitivity is measured by calculating the shift in cut off wavelength. The holes here are selectively infiltered. The band structure and the transmission spectra are obtained by finite

difference time domain and plane wave expansion method. Firstly, the first row of holes adjacent to the line defect is infiltered. This is repeated for various hole diameters. Next, infiltration is done for holes in the line defect. The device exhibits 5.3 times improved sensitivity.

F. Bougriou et al. [7] analyzed a highly sensitive liquid based sensor on a 2D photonic crystal waveguide. Here the radius of air holes adjacent to the line defect is increased and infiltered with ionized water (n=1.33). Finite difference time domain method is used to obtain transmission spectra. Wavelength shift of 270nm is observed giving a sensitivity of 818nm/RIU.

M. Doss et al. [8] designed a ring resonator with nano-photonic crystal which was studied for different structures. The crystals were of nano-meter size. Holes were removed from the rectangular and the hexagonal lattice in a three dimensional silicon slab. Finite difference time domain method was used to investigate the performance of the nano-ring resonator by varying the ring radius and the coupling distance.

M. Pu et al. [9] presented a refractive index based sensor on a photonic crystal waveguide with ring shaped holes. The shift in cut off wavelength is measured for different refractive indices and sensitivity is observed to be 110 nm/RIU.

T. Sunner et al. [10] studied the response of a photonic crystal to changes in the effective refractive index. The cavity was observed under different gaseous environments and pressures for which the transmission spectrum was calculated. It showed the linear dependence of wavelength on the refractive index of the gases. The high quality factor of the cavity leads to a shift in resonance by 8pm caused by a change in refractive index of 10^{-4} RIU.

X. Wang et al. [11] presented a highly compact gas sensor based on a 2D photonic crystal formed by a point defect in the resonant cavity. The refractive index is varied from n=1.0 to n=1.01 RIU and the transmission spectrums is calculated for each case. Lattice constant a=520 nm. The sensitivity is found to be equal to 433nm/RIU for a change in effective refractive index of 10^{-4}. Plane wave expansion method and finite

difference time domain method is used in this case. To observe the performance of the sensor theoretically the fabry-perot cavity mode is used.

R. Hao et al. [12] proposed a structure made up of two types of materials. One is the dielectric background (Si) and the other is inner dielectric rods (Zr_3N_4). These two materials are separated by air rings. Light of wavelength 1550nm is used with the ring radius r lying between r1 and r2. Silicon guiding layer is used on top of silicon oxide layer. A complete Photonic band gap with gap ratio of 7% is obtained.

A. Saynatjoki et al. [13] showed that the ring shaped photonic crystals (RPhCs) are more advantageous compared to conventional holes in photonic crystals (PCs). A larger band gap is obtained for RPhCs at low fill factors. They also showed that RPhC waveguides having high group index and a low group velocity dispersion can be further designed. The sensitivity is measured on the basis of a shift in cut off wavelength which was calculated for different refractive indices.

T. Hasek et al. [14] presented a photonic crystal waveguide used for fluid sensing application in the subterahertz range. A triangular array of air holes in a dielectric medium is produced on a two-dimensional crystal. Fluids with different refractive indices are inserted into the active region affecting the transmission characteristics in the stop band.

H. Kurt et al. [15] studied a two dimensional photonic crystal called annular photonic crystal which is composed of an array of circular air holes in a square or a triangular lattice with dielectric rods centered within each air hole. Despite the fact that the percentage of volume occupied by the dielectric rods is small (<12%), these dielectric rods modify the dispersion diagram of the photonic crystal. Because of the addition of dielectric material inside the unit cell, if we increase the radius of the dielectric rods from zero to a finite value, the band gap reduces and is closed completely. If we continue to increase the radius of dielectric rods above the finite value, another photonic band gap is obtained. If we compare the obtained dispersion diagrams with the original lattice consisting of circular air holes on a square/ triangular array in a dielectric background, the photonic band gap obtained for the new structure is

enhanced in size. The symmetry of the structure is preserved and a band gap is obtained at low normalized frequencies.

E. Snoeks et al. [16] proposed a square lattice of dielectric rods in air. The properties and existence of the photonic band gaps was investigated. To calculate the band structure transfer matrix method was used which is a function of dielectric constant of the rods and the radius –to- pitch ratio (r/a). For dielectric constants >3.8 (index contrast>1.95), band gap existed for transverse magnetic polarizations only. For small index contrast, r/a ratio is 0.25. The widest gap was observed in silicon rods for r/a=0.18. The effective index was obtained from the band structure and compared with the Maxwell–Garnett effective medium theory. Hence, the design parameters for silicon based photonic crystal waveguides were obtained from the band structure. Amorphous silicon, silicon germanium and silicon-on-insulator structures can be used to achieve index guiding in the third dimension. The possibilities and limitations of the same are discussed.

B.J. Luff et al. [17] used an integrated optical biosensor based on planar directional coupler and presented the measurements of bio molecular binding reactions. The device is fabricated in a glass by Ag+ –Na+ ion exchange. The sensing region is defined by the use of transparent fluoropolymer isolation layers which is formed by thermal evaporation. The sensor is suitable for the detection of environmental pollution.

S.R. Joshi et al. [20] discussed on the challenges that are faced by people suffering from diabetes in India. This disease is a major health problem prevailing in the country with over 40 million people suffering from the disease. The haemoglobin levels are 2% higher than the values which are suggested by the international bodies. In elderly patients, overaggressive treatments are considered to be highly dangerous. Hence, there is a need of proper awareness and proper control among the patients and doctors as well.

J. Nissl [21] discussed on the complete blood count method which provides us information regarding the number of RBC's, WBC's, and platelets in the blood. It

helps in checking symptoms such as weakness, fatigue etc. Various diseases such as anaemia, blood related infections, and many other disorders can be diagnosed.

Poonam Sharma et al. [23] designed a 2D photonic crystal for analysis of basal, cervical and breast cancer cells. The shift in wavelength was measured for normal and effected cells. FDTD method was employed for the analysis of these cells.

J. Zhang et al. [24] reviewed on the non invasive methods for detection of diabetes by measuring glucose levels. Instead of detecting the glucose levels in blood, he discussed about methods of detecting glucose in body fluids such as tears which is comparatively less painful.

P. Makaram et al. [25] also reviewed on non invasive methods of glucose detection using body fluids such as saliva, breath, serum, tears, urine which are an alternative to blood glucose measurements which are very uncomfortable and painful. He discussed about the nano-material based sensing techniques which are optimal due to their sensitivity and selectivity ranges.

Poonam Sharma et al. [32] designed a 2D photonic crystal waveguide for detection of different blood components such as blood plasma, glucose, white blood cells, red blood cells. FDTD method was employed for analysis. It was shown that with change in RI, there is shift in resonant frequency. Hence, the device acts as a sensor.

A.N Shvalov et al. [34] studied the light scattering properties of human erythrocytes. Scanning flow cytometer was used for experimental measurements in which polymorphism was observed for the measured light scattering pattern. Theoretically, Wentzel–Kramer–Brillouin approximation was used to study the pattern for different orientations. Comparison between experimental and theoretical results was done.

X. Xu et al. [36] investigated the optical properties of blood immersed in dextran which is a biocompatible agent. The optimal concentration required for optical imaging applications was found. Different molecular weights and concentrations of dextran were used and changes in light attenuation, refractive index, and aggregation

properties were studied. It was shown that the light scattering in the blood could be reduced with the application of dextrans.

M. Friebel et al. [39] determined the complex refractive index of highly concentrated haemoglobin in the wavelength range of 250 to 1100 nm using transmittance and reflectance measurements. The real parts of the complex RI's that were determined were 0.02 units higher than the ones in literature.

D.J. Wolf et al. [43] studied 117 cases of untreated basal cell carcinoma. The normal appearing skin which surrounded the tumor was marked in increments of 2mm. Mohs micrographic surgery was used to remove the tumor. The extent to which the tumor invaded was calculated from pre-surgical skin markings.

R. Kirchain et al. [47] discussed about the wide impact of nano-photonics and how it emerged as the new area in which the interaction of light with nano structured materials is studied.

B. Jalali et al. [48] discussed on why silicon seems to be the most appropriate choice for photonics industry. It discusses the various challenges that need to be faced before any large scale commercialization occurs. Silicon should be compatible and must operate within the thermal constraints of very large scale integrated (VLSI) chips that are used in CMOS technology. It discusses the optical properties of silicon in infra red range.

W. Bogaerts et al. [49] studied the fabrication techniques such as deep ultraviolet lithography using CMOS technology on SOI substrate. Photonic wires and photonic crystal waveguides are compared. With respect to propagation losses, it was shown that photonic wires perform better. For photonic wires, propagation losses obtained were 0.24 dB/mm and 7.5 dB/mm for waveguides.

P. Dumon et al. [51] demonstrated photonic wires fabricated through the process of deep UV lithography and dry etching with propagation loss equal to 2.4 dB/cm. Ring resonators having Q value of 3000 and low cross talk were also made.

A. Bazin [52] discussed on the designing, and fabrication of III-V semiconductor materials integrated with SOI substrate. Around 1.5 μm, III-V layer is patterned into a nano beam cavity. An adjustable coupling efficiency between the cavity and SOI substrate is obtained. Also, a continuous wave laser emission is obtained with a very low switching energy and an optical memory lasting more than 2 seconds.

C. Xiong et al. [54] discussed on the integration of aluminium nitride (AlN) films on silicon substrate. This work was done to obtain the active functionalities on a small chip. AlN was fabricated on SOI substrate with a very low propagation loss equal to 0.6 dB/cm. Utilizing very low energy consumption, an electro-optic modulation up to 4.5 Gb/s is obtained using Pockel's effect. High speed modulation at visible wavelengths is obtained.

C. Xiong et al. [56] discussed on how the integration of AlN on silicon substrate can be used for a wideband optical guiding. High quality optical and mechanical devices can be obtained. The process of achieving second harmonic generation in these photonic circuits is explained.

J. Arentoft et al. [59] discussed on the optical characterization of SOI waveguides. When an unpolarized light is passed through the waveguide, a very low insertion loss of 19 dB is obtained. A propagation loss of 4dB/mm is obtained using length mask technique.

M. Mulot [60] discussed about the 2D waveguides etched in indium phospide (InP) based materials. The entire fabrication and characterization process of PC structures etched in the InP/GaInAsP/InP is discussed. Ar/Cl_2 assisted ion beam etching is used for the fabrication purposes. For this entire system, a transmission loss of 10 dB/mm is obtained for a waveguide, a reflection of 96.5% is obtained for a 4-row mirror and a record quality factor of 310 is obtained for a 1D cavity. Optical filters were also demonstrated by inserting a Fabry-Perot cavity inside the waveguide. A coupling efficiency of 70% is achieved from a ridge waveguide to a line defect waveguide using a PC taper.

WHP Pernice et al. [63] designed AlN based nano cavities and high quality factors were obtained. Using a self protected process, these nano beams were fabricated in sputter-deposited AlN-on-insulator substrates. Quality factors up to 146000 were obtained. Extinction ratios in excess of 15 dB were obtained by varying the coupling gap between waveguide and cavity.

KSA Butcher et al. [66] reviewed on the latest advances in the physics of indium nitride (InN) and the related band-gap controversy. They examined the role of oxygen in the material. A 1.1–1.5 eV band-gap and an existing ~0.7 eV trapping centre are carefully examined. Nitrogen came out to be the newly discovered material and the supporting data related to this material is discussed.

The table below summarizes the main research papers that have been studied extensively for analyzing the work that has been done in the past in areas of photonic crystal waveguide based sensing applications.

S. No.	Name of author	Title of paper	Year of publish	Content
1.	C. Jamois	Silicon-based two-dimensional photonic crystal waveguides	2003	Discussed on the properties of silicon based two-dimensional photonic crystal, 2-D photonic crystals and slabs based on silicon-on-insulator basis.
2.	Yong Zhao, Ya-Nan Zhang, Qi Wang	Review on the Optimization Methods of Slow Light in Photonic Crystal Waveguide	2015	Discussed on various optimization methods to overcome the drawbacks related to slow light.

3.	Amit Kumar Goyal, Suchandan Pal	Design and simulation of high-sensitive gas sensor using a ring-shaped photonic crystal waveguide	2015	Proposed a ring shaped structure of holes in photonic crystal waveguides which can be used for gas sensing applications.
4.	Amit Kumar Goyal, Suchandan Pal	Design and simulation of high sensitive photonic crystal waveguide sensor	2015	Proposed a PCW based sensor in SOI material with circular holes. By varying the radius of the holes in the line defect and etch depth, the sensitivity values are measured. Average value of sensitivity obtained is386 nm/RIU.
5.	F. Bagci and B. Akaoglu	Enhancement of Refractive Index Sensitivity in Photonic Crystal Waveguide-Based Sensors by Selective Infiltration	2013	Presented a liquid based refractive index sensor. The first row of holes adjacent to the line defect is in filtered for various hole diameters. Next, infiltration is done for holes in the line defect.
6.	Dutta H, Goyal A K and Pal S	Sensitivity enhancement in photonic crystal waveguide platform for refractive index sensing applications	2014	Proposed a photonic crystal waveguide based sensor in silicon-on-insulator (SOI) material with circular holes. Ring shaped holes are

				introduced in the line defect. A wavelength shift of 210nm is obtained giving sensitivity of 420nm/RIU.
7.	Poonam Sharma	A Photonic Crystal sensor for Analysis and Detection of Cancer cells	2015	Designed a 2D photonic crystal for analysis of basal, cervical and breast cancer cells using FDTD
8.	C. Xiong, W.H.P. Pernice, and H.X. Tang	Low-Loss, Silicon Integrated, Aluminium nitride Photonic Circuits and their use for Electro-optic signal processing	2012	Discussed on the integration of AlN films on silicon substrate. to obtain the active functionalities on a small chip.
9.	J. Arentoft, T. Sondergaard, M. Kristensen, A. Boltasseva, M. Thorhauge, and L. Frandsen	Low-loss silicon-on-insulator photonic crystal waveguides	2002	Discussed on the optical characterization of SOI waveguides obtaining an insertion loss of 19 dB and propagation loss of 4dB/mm.

Table 1: Summary of work done in the past in field of PCW based sensing applications

CHAPTER 3

RING SHAPED PHOTONIC CRYSTAL WAVEGUIDE FOR GAS SENSING

In this chapter, we have discussed about a sensor designed using ring shaped holes that is used for sensing various gases. As compared to circular shaped holes, ring shaped holes have been used to measure the enhancement in sensitivity. Transmission spectrum is calculated for various hole diameters in order to see the effect of increase in hole diameter on light transmission. Further, we see this effect of increase in hole diameter on sensitivity. Structure is optimized by etching these holes in the silicon layer and further etching in the buried substrate layer. At the end, infiltration of various gases is done to measure the overall sensitivity of this structure. The design is based on shift in peak resonant wavelength which is obtained due to change in RI of various analytes. This changes the sensitivity values as obtained by the formula discussed in the below sections.

3.1 REFRACTIVE INDEX BASED GAS SENSORS

Gas sensors based on refractive index change can be categorized into bulk PCs, PCWs and PC cavities [6]. In case of cavity based sensors, even a small sensing area can bring a change in sensitivity. Changing the defect size leads to change in resonant frequency, leading to a change in sensitivity. However, they are difficult to fabricate. In comparison, PCWs can be fabricated easily.

Change in the geometrical parameters such as holes shape and size leads to a change in sensitivity as measured by the shift in cut off wavelength. These holes can be etched up to a finite depth in the dielectric material leading to a change in the optical properties of the structure. Also, infiltration with analytes of different refractive indices leads to variation in sensitivity values which is again measured by the shift in cut off wavelength. This row of holes responsible for the change in the properties of the crystal forms the line defect. Analyte infiltration leads to a change in the effective

refractive index of the guided mode. Hence, the output transmission spectrum changes accordingly.

3.2 GAPS IN THE PREVIOUS WORK

This section lists the common limitations encountered in the previous work done by the researchers.

- In the conventional photonic crystals, described by an array of circular holes, transverse electric field polarization is obtained in which it is quite difficult to achieve full band gap.
- The previous structures are very difficult to fabricate because the behaviour of the crystal changes even with a small change in any of the parameters of the structure.
- Also, these structures have lower sensitivity values.

Research has been done in the field of annular photonic crystal which was formed by placing dielectric rods within air holes in the centre. This type of photonic crystal was found to be polarization independent. The band gap obtained was also polarization independent. This concept was used to obtain highly sensitive gas sensors.

A photonic crystal micro-cavity based gas sensor of sensitivity 433 nm/RIU (refractive index unit) has been reported by Wang et al. [11]. Sunner et al. also designed a photonic crystal based cavity structure and reported a shift in resonance wavelength by 8 pm with a change of refractive index by 10^{-4} RIU [10].

So, to improve the sensitivity values, a new structural design for refractive index based gas sensor is needed.

3.3 RING SHAPED PHOTONIC CRYSTAL WAVEGUIDE

Here, we design a refractive index based gas sensor based on a 3D photonic crystal waveguide that is formed by using ring shaped holes as compared to conventional

circular shaped holes used in previous studies. We use SOI substrate in which silicon is considered as the guiding layer and silicon oxide is buried underneath the silicon layer. To transmit the required input wavelength, we incorporate defects in the structure. These holes are further etched up to a finite depth in the oxide layer for optimization of our structure. Fig 10 below shows ring shaped holes with outer diameter D and inner diameter d.

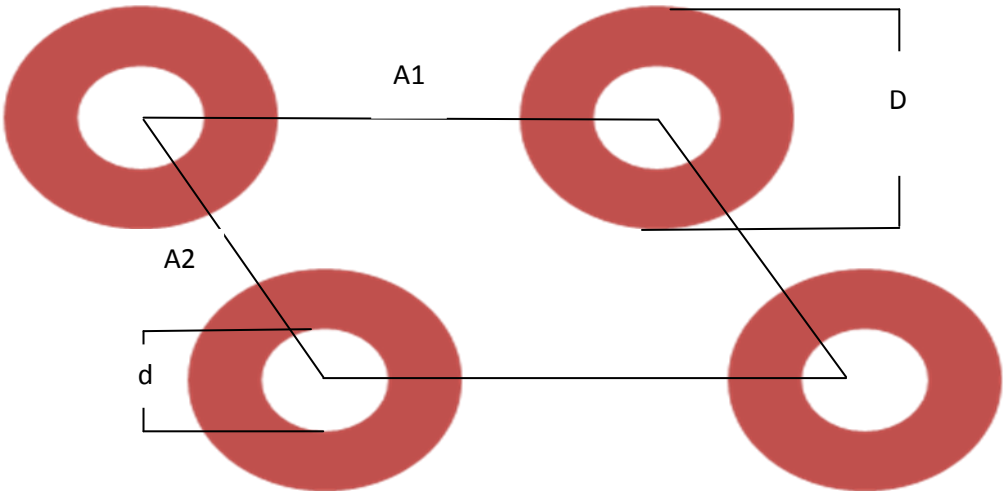

Fig 10. Ring type structure in a photonic crystal waveguide

A1	Lattice constant1
A2	Lattice constant 2
D	Outer hole diameter
d	Inner hole diameter
(D-*d*)/2	Ring thickness

Table 2: Parametric description of ring shaped photonic crystal waveguide

3.4 WORKING PRINCIPLE

As explained in Chapter 1, photonic crystals are materials in which the refractive index varies periodically. The associated band gap property is such that signals lying within a particular frequency range are not allowed to pass through the crystal. However, defects are introduced in the material so that signals that lie within a certain frequency range are allowed to pass through. These defects may be line or point defects. Using this band gap property, photonic crystals can therefore be used to sense different analytes. With the change in the refractive index of the analytes, the effective index of the slab changes, leading to a shift in the cut off wavelengths. Thus sensitivity can be measured and is normally expressed as:

$$S = \frac{\Delta\lambda}{\Delta n} = f\,\frac{\lambda}{n} \tag{26}$$

$\Delta\lambda$ is the change in cut-off wavelength,
Δn is the change in refractive index of the analyte,
n is the refractive index of the slab,
λ is the input wavelength transmitted,
f is the defect filling factor

Equation (26) shows that the shift in wavelength is proportional to the filling factor i.e., the area that is available for sensing. Hence, sensitivity increases with the increase in filling factor.

The defect filling factor is expressed as:

$$f = \frac{\pi}{2\sqrt{3}}\left(d/a\right)^2 \tag{27}$$

Here, *a* is the lattice constant and *d* is the defect hole diameter.

It can be seen from equation (27) that the response of our structure is related to hole diameter *d*. Hence defect filling factor is also known as response factor.

So, sensitivity changes with the change in refractive index of the analytes, due to shift in the cut off wavelength.

3.5 GAS SENSOR DESIGN

In this section, we consider a 3D photonic crystal waveguide with silicon-on-insulator (SOI) wafer. Silicon forms the guiding layer. For improvement of sensitivity compared to previous studies, we consider ring shaped holes. Silicon oxide is the substrate in this case which lies beneath the silicon layer. For optimization purposes, ring shaped holes are etched in the silicon layer. Thickness of silicon layer is considered to be 0.220 μm. The lattice constant is taken to be 0.5. Outer hole radius which represents air in silicon is taken to be 0.21 μm and radius of inner hole representing silicon in air is taken as 0.11 μm. We set the thickness of the substrate to a large value so that it extends beyond our simulation domain. The entire simulation is done using FDTD software tool. Here, the refractive index of silicon is taken as 3.46. The upper cladding represents air having refractive index=1, and the lower cladding represents silicon oxide having a refractive index=1.414. Ring has a refractive index same as that of silicon layer.

Fig 11 below shows our designed structure. We then remove a single row of holes from the middle of structure in the Γ-K direction in order to obtain a photonic crystal waveguide as shown in Fig 12. Band gap is obtained around 0.3532-0.36628 a/λ (Fig 13). From this we find that an input wavelength of around 1450 nm can be transmitted through the crystal. This is obtained once we introduce defects in our crystal.

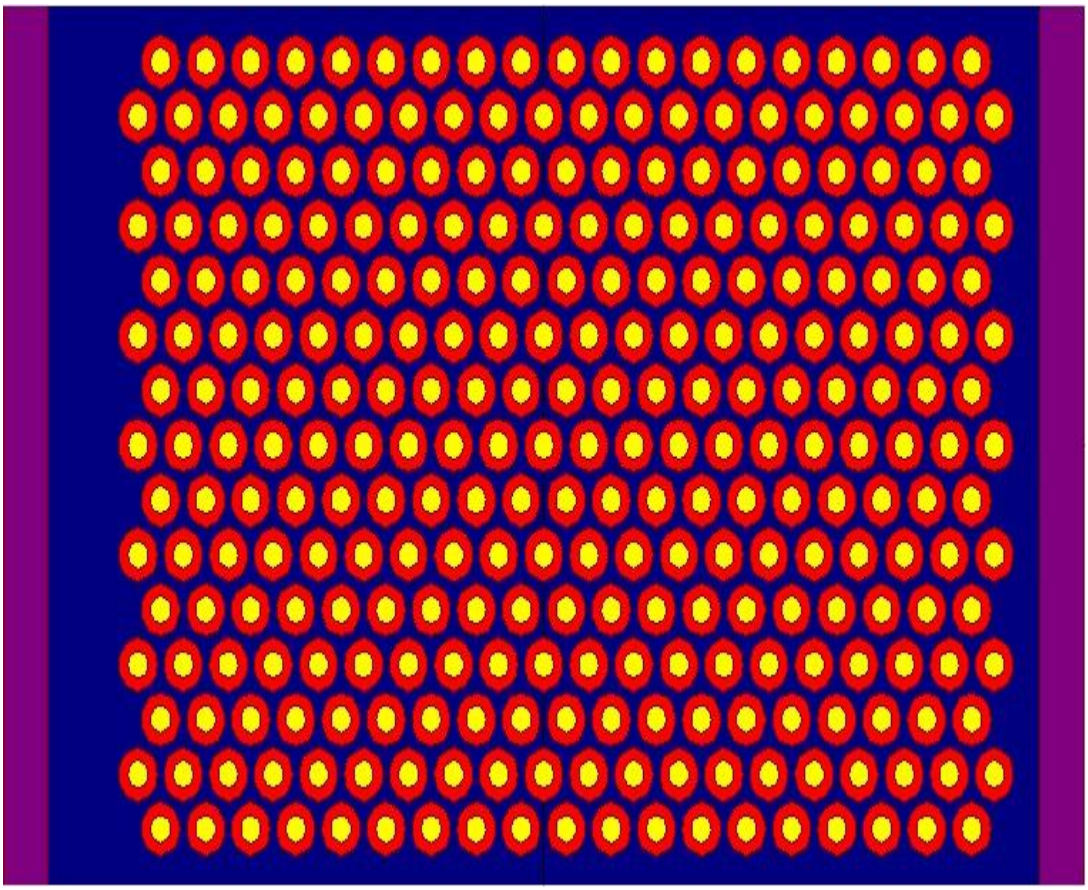

Fig 11 Photonic crystal structure with ring shaped holes on SOI wafer with lattice constant=0.5

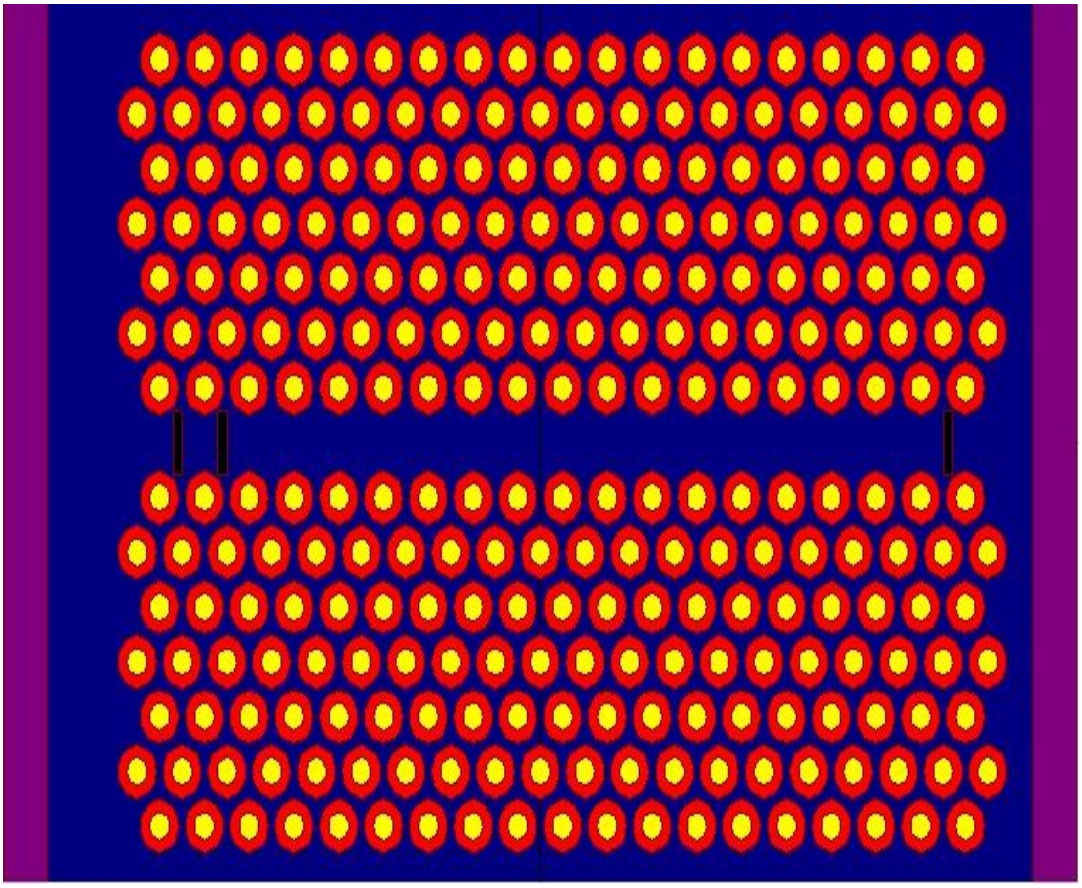

Fig 12 Photonic crystal waveguide as obtained by removing a row of holes in the Γ-K direction

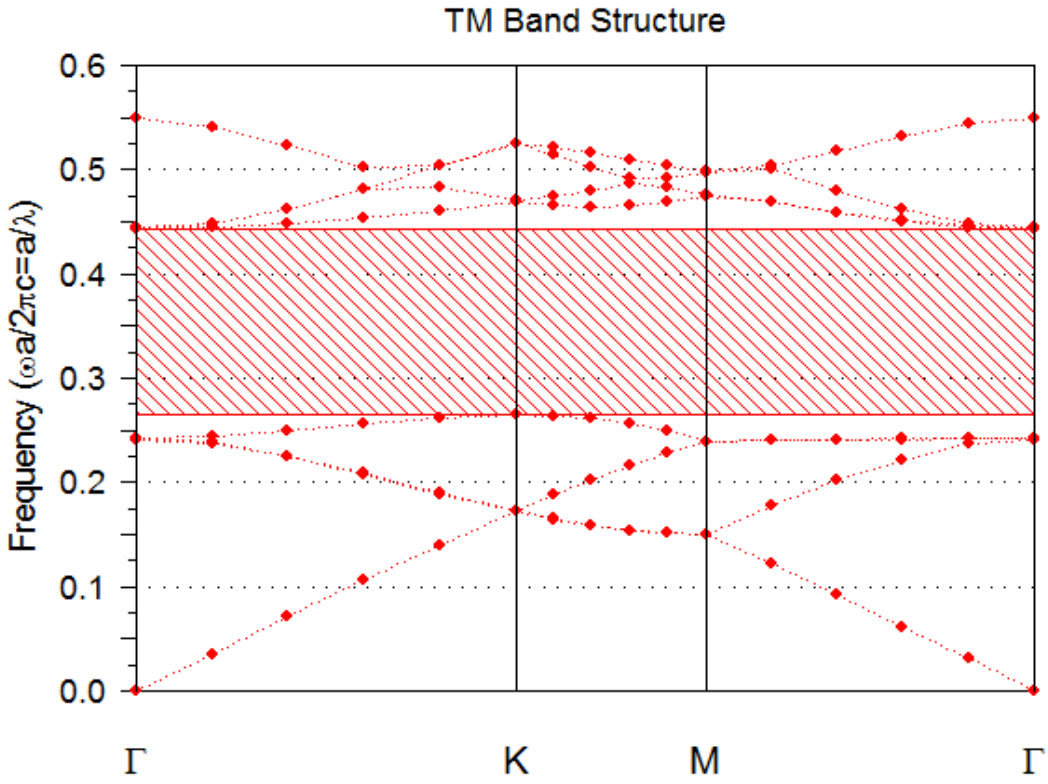

Fig 13 Band structure as obtained by removing a row of holes from the middle

3.6 RESULTS AND ANALYSIS

Earlier we have removed a row of holes from the middle in order to find out the input wavelength that needs to be transmitted through the crystal. Now, we introduce a new row of holes which are circularly shaped and have a smaller diameter as compared to the ring shaped holes used in the structure. This leads to an enhancement in sensitivity as obtained by shift in resonant wavelength. This happens because with the introduction of new holes, fill factor in our sensing region increases. Intensity of electromagnetic waves increases, because of increase in the light matter interaction in our crystal. Hence, there is a considerable increase in sensitivity. However, there is a decrease in effective refractive index of the structure. Fig 14 shows this process.

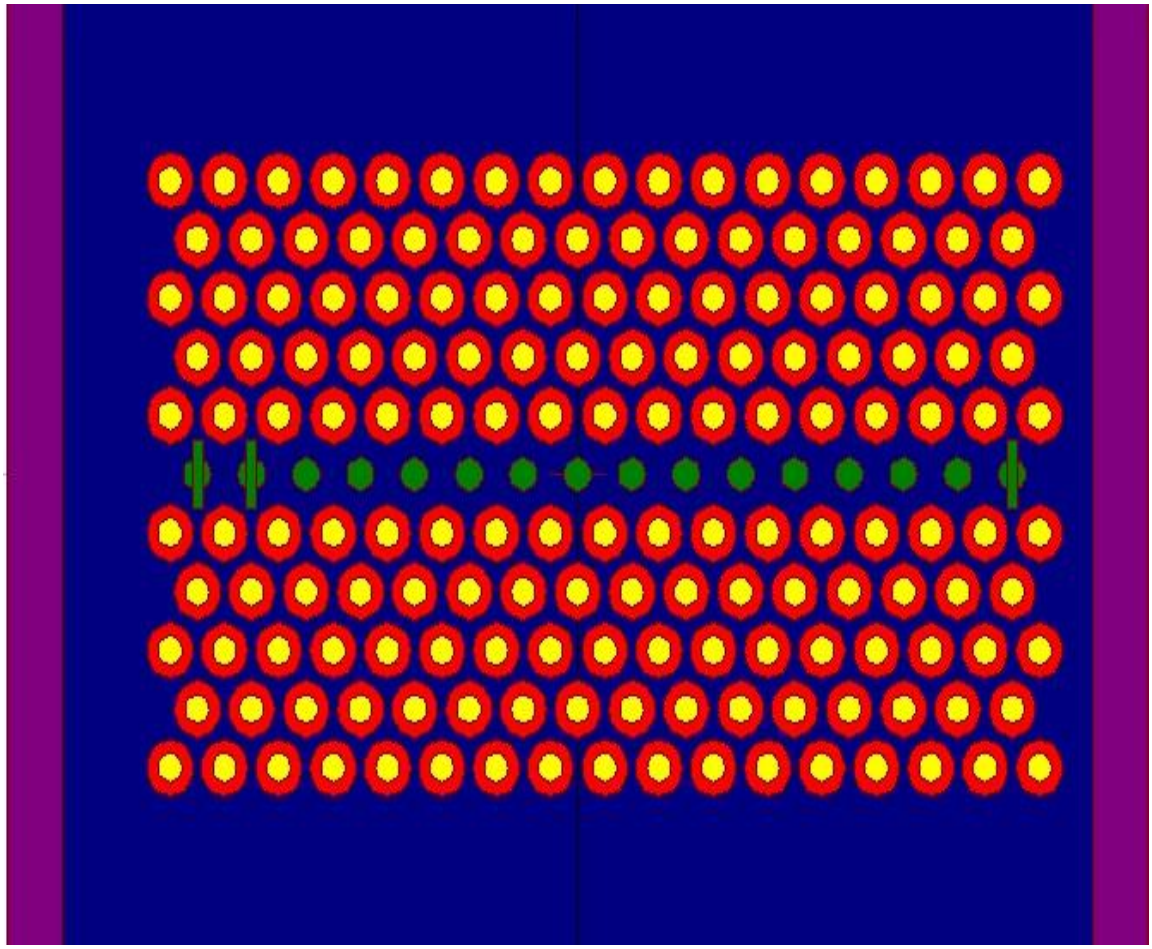

Fig 14 Photonic crystal waveguide showing the line defect obtained by introducing a new row of holes.

For this new row of holes introduced as part of line defect, diameter is increased from 0.25 µm to 0.30 µm. It is observed that with the increase in the holes diameter, transmission gets affected after we analyze the transmission spectrum in 3D FDTD. As the guided modes get converted into leaky modes, the range of the forbidden band gap increases, which leads to a reduction in strength of the transmitted signal. Hence, transmission spectrum cannot be detected beyond the defect diameter of 0.27 µm.

There is a decrease in the intensity of light as it travels through the waveguide. Fig 15 shows the effect of increase in diameter of holes on light transmission.

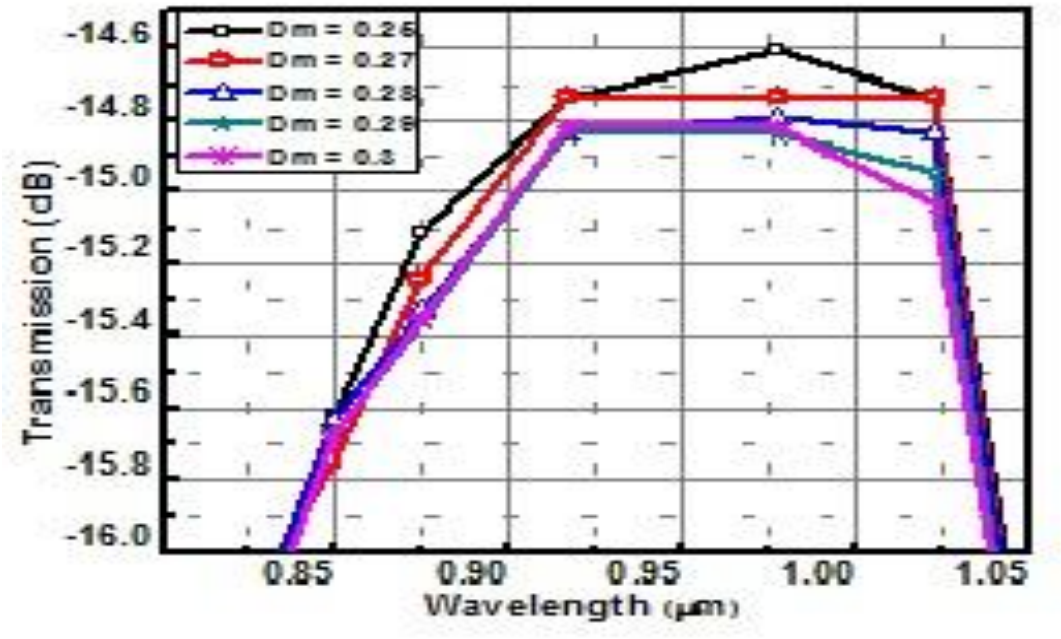

Fig 15 Effect of increase in hole diameter on the transmission spectra
Series 1 to 5 represents the diameter varying as 0.25µm, 0.27µm, 0.28µm, 0.29µm and 0.30µm respectively.

As explained above, introduction of new row of holes leads to increase in fill factor near the waveguide. Because of this, there is change in the effective refractive index which leads to an increase in the sensitivity with the increase in defect diameter. The sensitivity increases from 285nm/RIU to 410nm/RIU as shown in Fig 16.

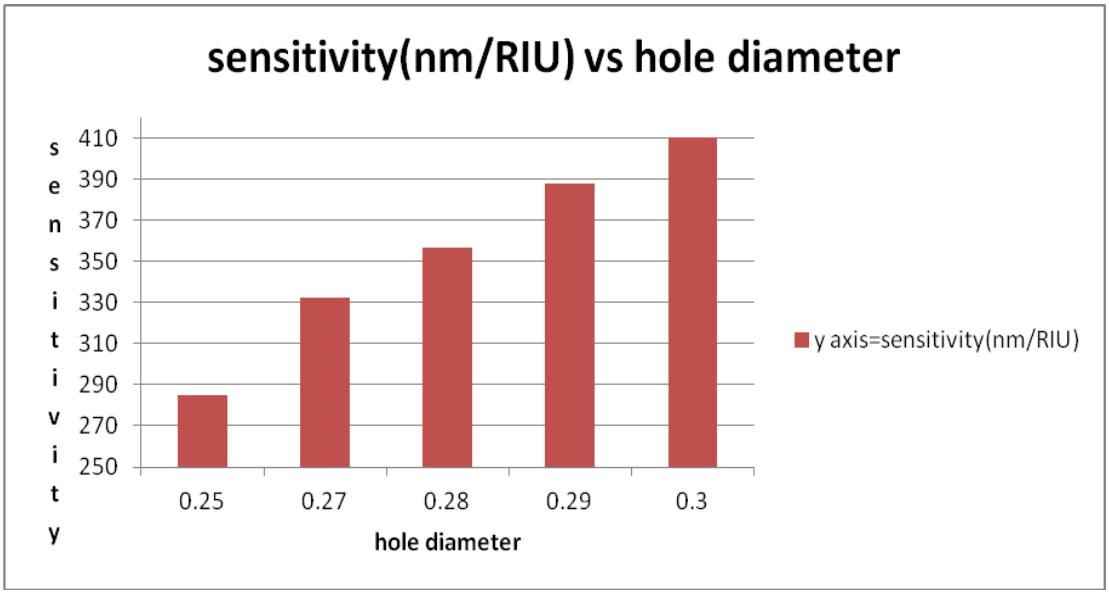

Fig 16 Change in sensitivity with the increase in defect diameter.

We further optimize the sensitivity by two processes: firstly, we etch the holes in the silicon guiding layer. Next, we over-etch these holes in the buried oxide layer in order to obtain a further improvement in sensitivity. This happens because there is an increase in the index contrast as obtained by etching the holes up to a certain finite depth. This etching profile is shown in Fig 17 and 18.

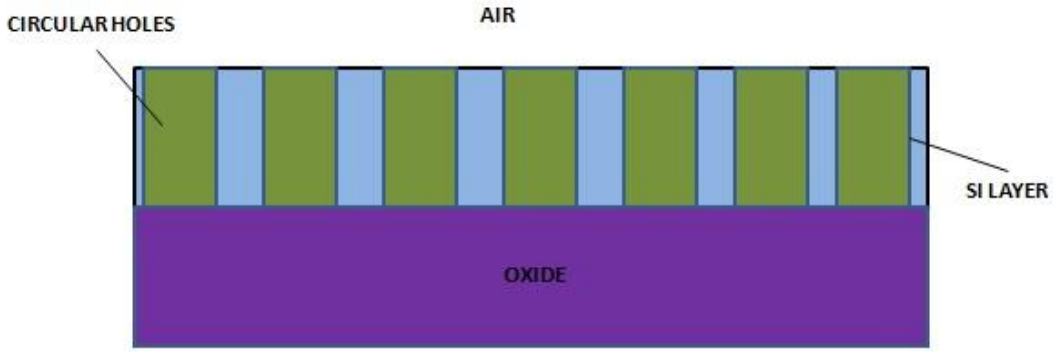

Fig 17 Etching of air holes in the silicon layer.

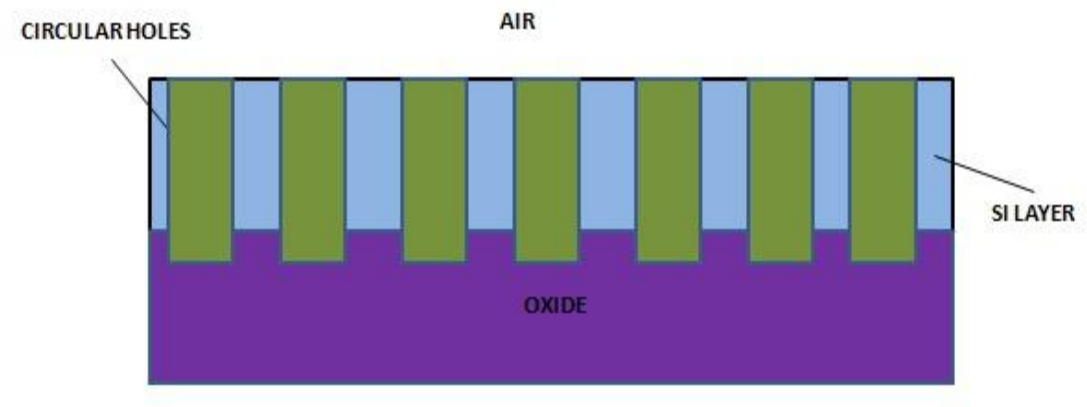

Fig 18 Etching of holes up to a certain finite depth in the silicon oxide layer.

This increase in sensitivity due to etching happens because there is better and effective guiding of light through the waveguide. This leads to an increase in the guiding mode energy. However, in PCW there is less guiding mode energy in the buried oxide layer. The structure parameters remain fixed as described earlier for this process. The lattice constant, inner and outer radius is fixed at 500nm, 110nm and 220nm respectively. As described in Fig 15, there is no effective transmission beyond the defect hole diameter of 270nm. So we fix this diameter to this value for further simulation. The transmission spectrum is shown in Fig 19 below.

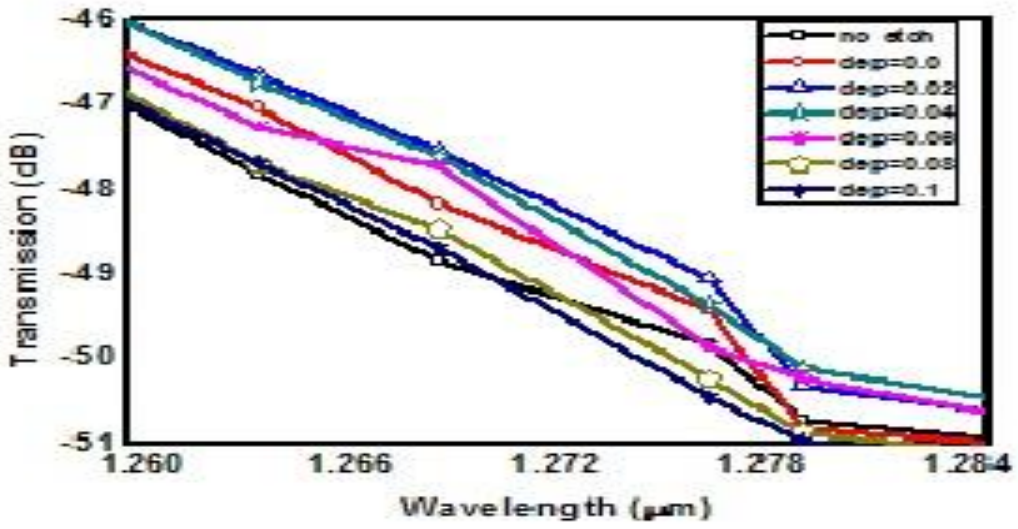

Fig 19 Effect of etching on transmission spectrum

It can be seen from the above figure that transmission losses increase beyond the etch depth of 0.04 µm in the buried oxide layer. Hence sensitivity decreases. So, up to an etch depth of 0.04 µm it increases, after which it is found to be decreasing.

Next, we analyze enhancement in sensitivity by the infiltration of various gases inside our structure. By using different gases of varying refractive indices, we observe that there is a shift in cut off wavelength as obtained by the change in refractive index inside the structure. Fig 20 below shows the output transmission spectrum obtained for various gases. The parameter values are fixed same as above (Hole diameter=0.27µm, lattice constant=0.5µm) for this simulation also. The etch depth is now fixed to 0.4 µm in the silicon oxide layer.

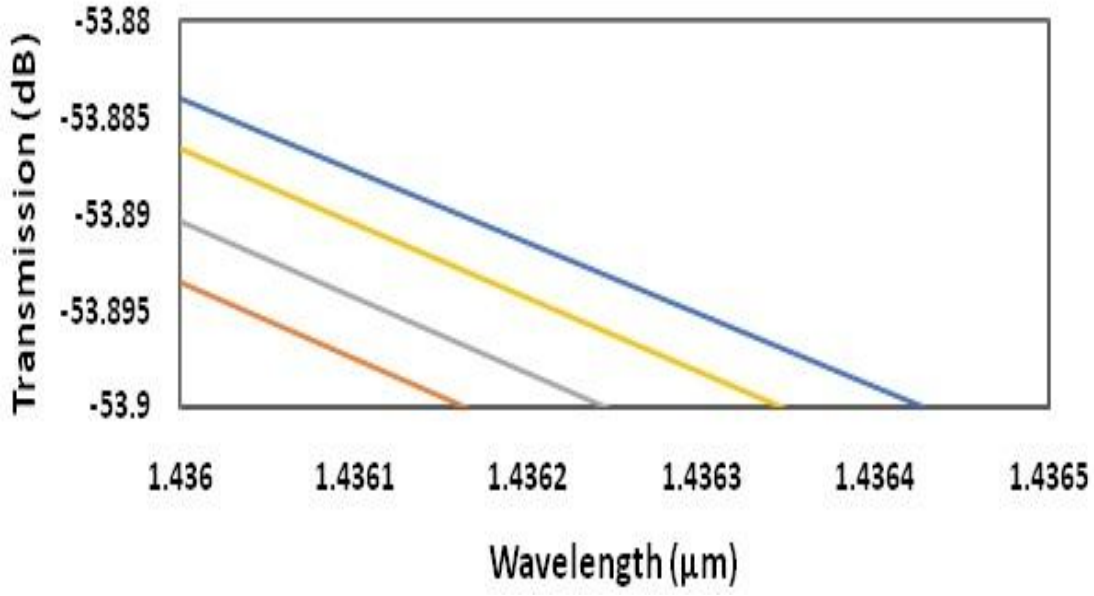

Fig 20 Output transmission spectra obtained by the infiltration of different gaseous analytes.

Fig 21 shows the plot of shift in cut off wavelength obtained by the change in refractive index inside the crystal. For refractive index change from 1.000 RIU to 1.0004 RIU, sensitivity is obtained to be 675 nm/RIU.

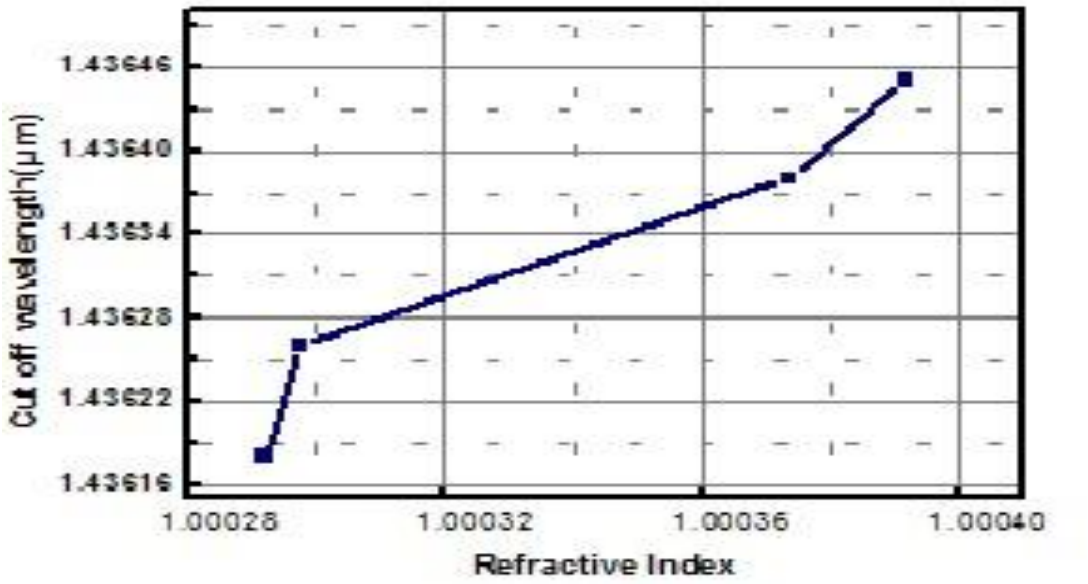

Fig 21. Shift in cut off wavelength obtained by the infiltration of different gaseous analytes

CHAPTER 4

PHOTONIC CRYSTAL WAVEGUIDE FOR DETECTION OF DISEASES

In this chapter, we focus on designing a bio-sensor based on photonic crystal waveguides for sensitivity and quality factor measurements. Because of the use of diverse technologies and methods, a bio sensing device can be defined in many ways and can find a wide variety of applications. M. Cooper defined bio sensor as a device which can be used to detect analytes or molecules with the use of chemical or biological receptors in a sample. S.P.J Higson defined bio sensor as a chemical sensing device which can be used for quantitative measurement of bio-chemical parameters. So in general, a bio-sensor is a system which is used to detect some analyte which binds to the bio-chemical layer. This binding mechanism is used to get a desired signal which can be analysed for various parameters.

4.1 OPTICAL TRANSDUCERS

When light interacts with the target molecules, the signal to be measured is obtained. When a variation in physical or chemical parameter is produced in the structure, there is change in the effective RI of the propagating mode. This forms the basis of sensing mechanism. Whenever a wave travels through the core of a waveguide, there is decrease in its intensity, as a fraction of its energy extends in the surrounding environments. This is the main reason for change in effective RI of the propagating mode. Some amount of this wave travels on the surface, while some travels inside the core. Therefore, the design parameters play an important role in deciding the performance of the sensor. Fig 22 shows the schematic of a bio-sensor showing the interaction of light with analytes.

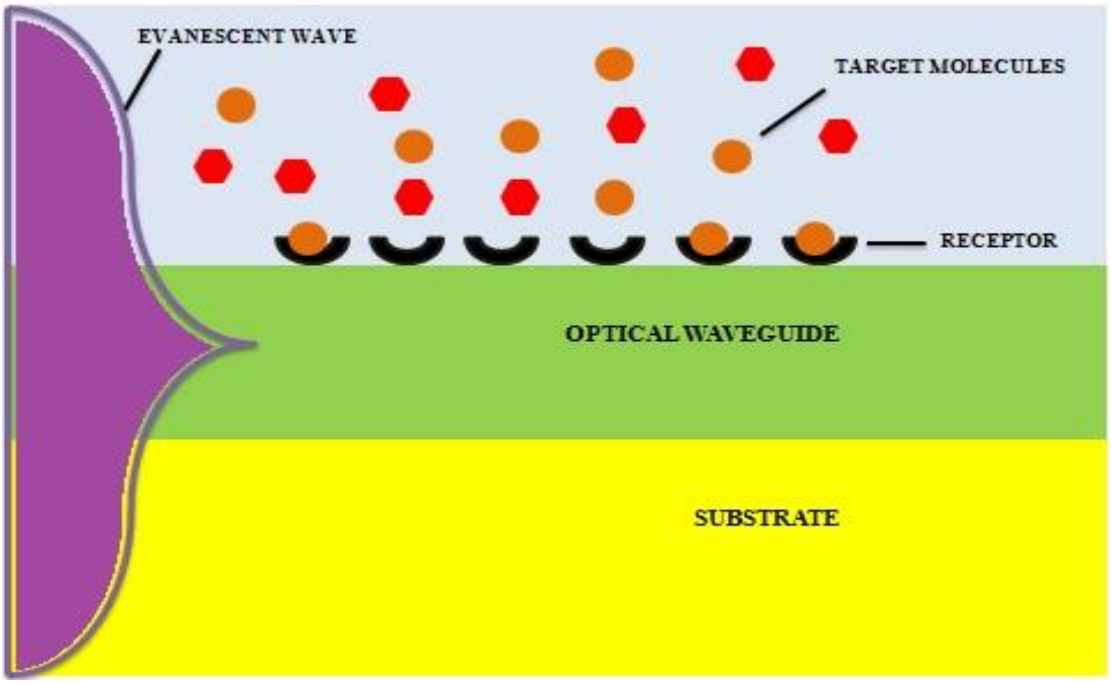

Fig 22 Schematic of a bio-sensor showing the interaction of light with molecules

4.2 BIO-SENSOR FOR DETECTION OF DISEASES

In this section, we have presented a 2D photonic crystal waveguide based biosensor for detection of different components in blood such as red blood cells, white blood cells, blood plasma, haemoglobin, and biotin-streptavidin. Further, we exploit this sensor to differentiate between normal and cancerous cell lines for the detection of basal cancer, breast cancer, and cervical cancer. The sensor can also be used to detect a person with or without diabetes by using tear as the analyte. Entire mechanism is based on the shift in peak resonant wavelength as discussed in Chapter-3 obtained by the change in refractive index of the analyte used for sensing.

Discussed below are some of the common diseases which are prevailing in our society and are the main causes of death all around the globe. The earlier these diseases are detected, better are the chances of cure.

- ***Cancer:*** Cancer or malignancy is caused due to abnormal growth in the body cells. Breast cancer, cervical cancer, lymphoma, basal cancer, lung cancer are the most common. According to an estimate, in 2016, there will be 1,685,210

new cancer cases diagnosed and 595,690 cancer deaths in the US [18]. Common symptoms related to cancer include fatigue, weight loss and fever. These occur as most of the body's energy supply is used by the cancer cells and they change the way a human body uses food for energy. As it grows, it pushes to nearby organs, nerves, vessels etc [18]. If diagnosed at an early stage, more than 9 in 10 bowel cancer patients will survive the disease for more than 5 years. More than 90% of women diagnosed with breast cancer at the earliest stage survive their disease for at least 5 years compared to around 15% for women diagnosed with the most advanced stage of disease [19]. Echocardiogram, MRI, colonoscopy, computed tomography scan are some of the conventional methods of early detection.

- ***Diabetes:*** According to WHO, 246 million people in the world are living with diabetes [20]. When the insulin production in the body is inadequate or the body's cells do not respond properly to insulin, the blood sugar level increases leading to diabetes. Patients suffering from diabetes experience frequent urination, they become increasingly thirsty and hungry.

- ***Blood disorders:*** Blood is a liquid with numerous cells and proteins providing nutrition and oxygen to the body and provides removal of wastage from the body. Blood is composed of blood cells such as red blood cells (RBC's), white blood cells (WBC's), platelets and blood plasma. Leukemia, hemmorhage, lymphoma, anaemia, malaria are some of the blood related disorders. Some of the common blood tests include blood count, blood smear, bone marrow biopsy, coombs test [21].

The conventional techniques used for detection of diseases are time consuming and painful. Also the equipments required are bulky and expensive. As compared to these conventional methods, recent technologies have revealed that modern biosensors are more effective in terms of time and cost. These biosensors exploit nano- or micro-fabrication technologies and use of optical, mechanical, electrical transducers. As discussed above, biosensor is a device which is used to detect the analytes or molecules of a sample by means of a binding mechanism.

Researchers from Rowan University detected Parkinson's disease at an early stage by using human protein microarrays in order to identify blood-borne antibodies which act as potential biomarkers in the detection process. This happened with with an overall accuracy of 87.9 percent. In the process of differentiating between early and mild-moderate stages of the disease, an accuracy rate of 97.5 percent is achieved [22]. By using bio-sensor as a device, target cell lines or changes in protein contents of cell have been analyzed in cancer research [23]. Patients suffering from diabetes have to draw blood in order to test the blood glucose level, which is painful and causes discomfort. Glucose can be tested using tear fluid which is rather attractive as in is easily accessible than blood and less painful [24]. The detection limit is low (since glucose is present in tear fluid at levels of 50–100 times lower than in blood), plus it is highly selective and small volumes can be measured in short durations of time [25]. In 2011, a highly sensitive sensor has been investigated by Yan et al. This sensor has very low detection limits of glucose in the range of 1.5 ± 0.4 μM which was enough to measure tear-fluid glucose levels, with a glucose sensitivity of 0.032 ± 0.02 nA/μM [26].

As we've earlier discussed, photonic crystal waveguide based biosensors are highly promising platform to develop lab-on-chip devices. They are highly sensitive, highly selective, and can be easily integrated or fabricated with other electrical components. They have the potential for fast and effective recognition of DNA, proteins, bio-molecules for the early diagnosis of diseases [23].

The band gap property of photonic crystals make them effective for various sensing applications such as bio-sensors to detect the specific binding between the target receptor bio-molecules on a suitable substrate with probe bio molecules in the sample solution [29].

4.3 BIO-SENSOR DESIGN

PCW design in this chapter consists of a hexagonal array of silicon (RI=3.45) rods in air (RI=1) on top of an oxide layer. The thickness of silicon rods is considered to be 220 nm. We consider the lattice constant of the structure as 410nm and the radius of silicon rods as 120 nm. The structure is supposed to be composed of two waveguides- a bus and a drop waveguide and a diamond shaped ring resonator. By reducing the radius of silicon rods to 30 nm, line defect is introduced in the bus and drop waveguide regions and a diamond shaped ring resonator. Through the bus waveguide, input light is introduced into the structure and at the drop waveguide, output is monitored. Photonic band gap occurs around 0.6174-0.7820 $1/\lambda$ giving the wavelength range of 1278-1619nm that can be transmitted through the crystal. Hence, the centre wavelength is taken as 1550nm. As shown in the figure below, a ring-shaped cylinder with outer radius (R) equal to 200nm and inner radius (r) equal to 180nm is considered in the middle of diamond shaped resonator. Sensing mechanism is applied in this area. The process consists of filling the inner hole of the ring shaped middle cylinder with the corresponding analyte in order to observe the shift in refractive index. The design of the biosensor is shown in Fig 23 below.

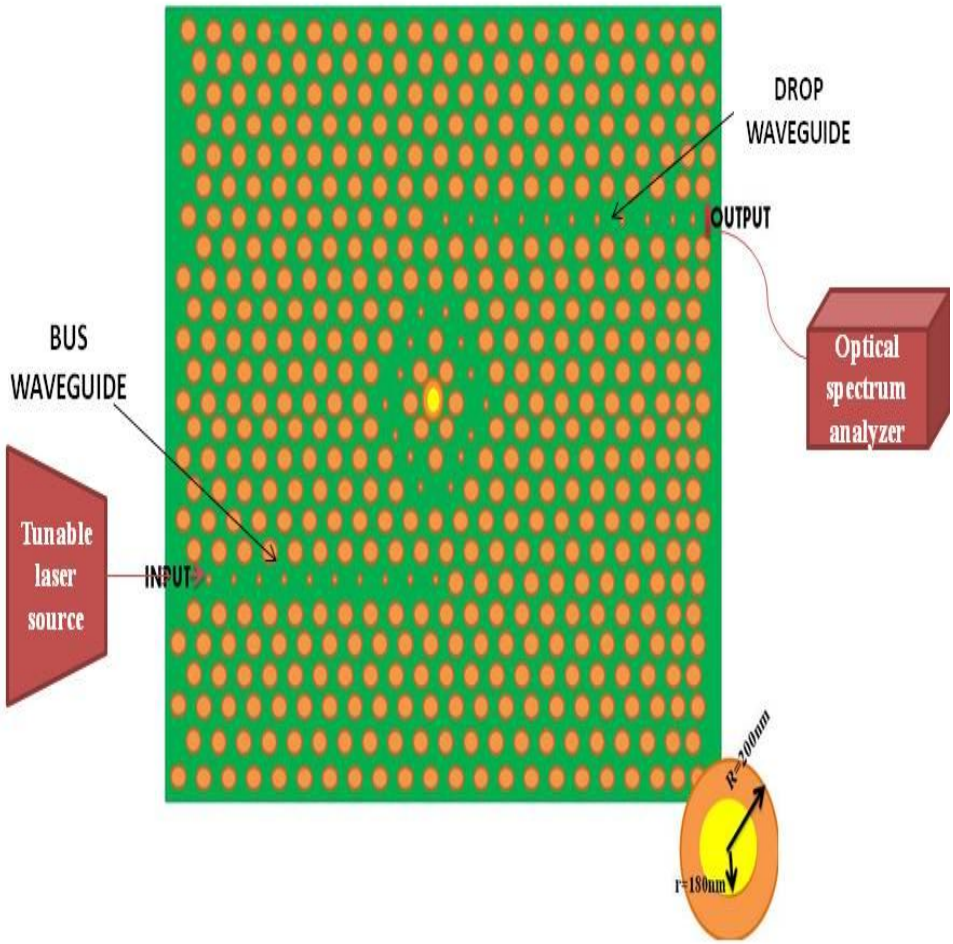

Fig 23 Design of the photonic crystal waveguide based bio-sensor. The structure consists of two waveguides-a bus and a drop Waveguide.

4.4 RESULTS AND ANALYSIS

At the input, continuous wave is launched and at the output, time monitor is used to get the transmission spectrum.

Atago's digital hand-held refractometer is used for calculation of analytes refractive indices with a measurement scale in the range of 1.3306 to 1.5284 [30]. Scanning flow cytometer [31], scattering [32] and optical coherence tomography [33] are some other methods that can be used for refractive index calculations. The above method of refractive index calculation is comparatively easier, inexpensive, portable and rapid results can be obtained. For zero setting purposes, water (RI=1.33) is initially used as the base analyte. After this, the respective analyte is placed on the prism of the refractometer for corresponding refractive index calculations.

For blood related diseases, various components in blood such as blood plasma, red blood cells (RBC's), white blood cells (WBC's), haemoglobin, etc are detected here. The process of density gradient centrifugation is used to separate these components first. In this process, separation occurs such that at the base, heaviest particles or the highest concentration (RBC's in this case) is obtained and at the top of the flask, the lowest concentration is obtained (blood plasma) [34]. The separation of various components in the blood as obtained by this process is shown in Fig 24.

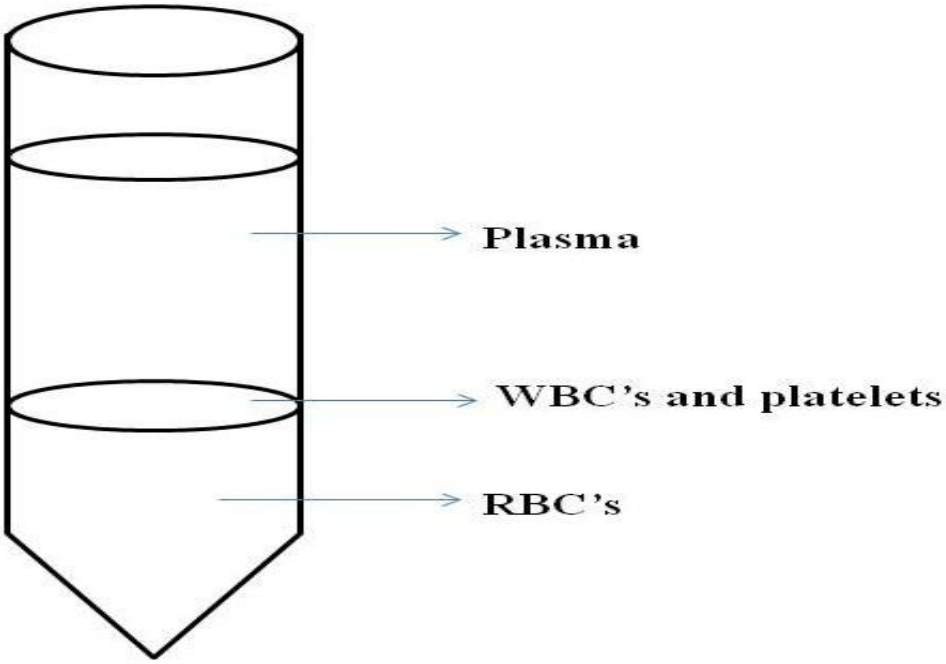

Fig 24 Separation of blood components obtained by the process of density gradient centrifugation

By using Atago's refractometer, with water as the reference analyte, and further using these components as analytes, we find their corresponding refractive indices.

- ***Biotin-Streptavidin:*** Biotinylation is the process in which biotin binds itself strongly with any molecule or protein. This process does not change or disturbs the molecule in any form because biotin is very small in size. This binding is highly resistant to high temperature or pH conditions. Hence it can be used to study protein-protein interactions that are highly sensitive in nature and is exploited in the areas of bio-technology for protein detection [35]. The biotin-streptavidin system obtained has a refractive index value of 1.45 [36].

- ***Haemoglobin:*** Haemoglobin carries oxygen from the lungs and returns carbon-dioxide to the lungs. It is the main component of the blood that carries oxygen throughout the body by binding itself to oxygen. More the binding, more is the amount of oxygen available in our body. It can be used for detecting thalassaemia and anaemia in the body with a refractive index value of 1.38 [36].

- ***Blood Plasma:*** It is mainly composed of water. The food we eat is composed of various nutrients. It is the plasma which carries these nutrients throughout the body. Plasma is responsible for carrying the waste products from the body cells to the kidneys and can be used for the detection of cardiovascular diseases [37]. Its RI value is equal to 1.35 [36].

- ***Red Blood Cells:*** As mentioned above, haemoglobin which is the main component of RBC's is used to carry oxygen inside our body. RBC's are also used to remove carbon dioxide from the body. For build up of healthy RBC's inside blood, iron and vitamins are required. Lack of iron causes a condition called anaemia in which there is no proper transportation of oxygen throughout the body. It has a refractive index value of 1.40 [38].

- ***White Blood Cells:*** The component of immune system responsible for protecting the body against various kinds of infections including bacterial or fungal, parasitic. They defend our body against cancer cells. In comparison with RBC's they can easily move in and out of blood vessels. WBC's having a refractive index value of 1.36 [38] and can be used for detection of congenital disorders, diminished bone marrow function, and drugs inside our body [39].

By using these blood components as the test analyte, the transmission spectra obtained is shown in Fig 25 below. As it can be seen from the figure, with the increase in RI values, the graph shifts toward right.

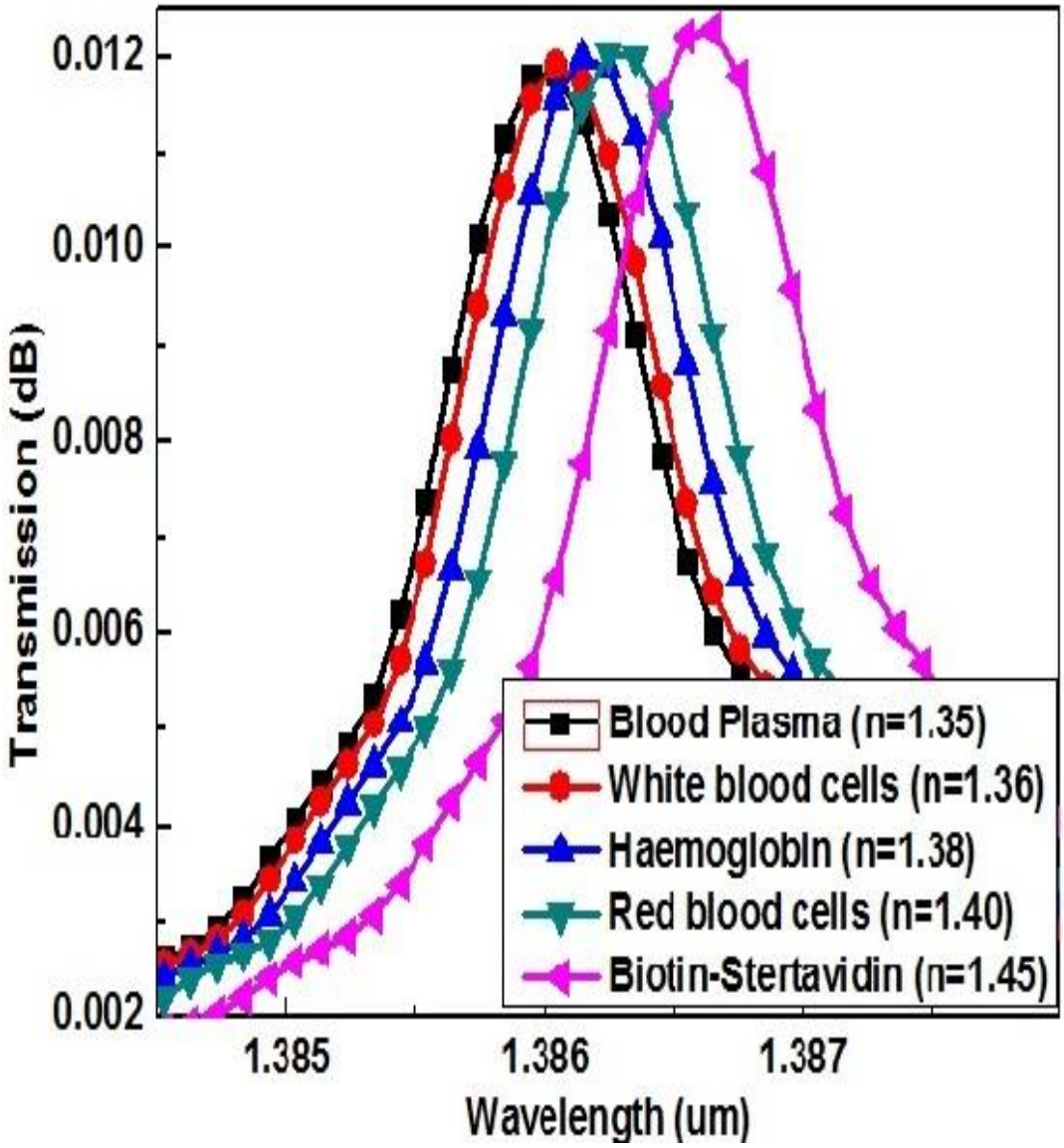

Fig 25 Output transmission spectra obtained for various blood components

The design is further used to differentiate between normal and tumor causing cell lines inside our body.

- ***Basal cancer cell***: It arises in the outermost layer of the skin (epidermis) and is caused by intense exposure of the skin to the sun. This causes damage of DNA inside the skin [40]. These cells do not spread to other parts of the body. Hence it is the least risky cancer amongst all. It has a refractive index of 1.38 and normal basal cells have a refractive index of 1.36 [41] [42].

- ***HeLa cancer cells***: These are human cervical cancer cells and were the first type to be cultured continuously for experiments. They multiply in an uncontrolled way as compared to normal cells. These cell lines were derived after biopsy was carried out on a poor 31-year old lady named Henrietta Lacks who was suffering from cervical cancer. These cell lines became cancerous due to infection with human papilloma virus 18 (HPV18) [43]. They have a refractive index of 1.392 whereas the normal HeLa cell line has a refractive index of 1.368 [44] [45].

- ***MDA-MB-231***: It is extracted from the human breast. Its isolation was done from pleural effusions of a breast cancer patient [46]. It has a refractive index of 1.399 and normal breast cell line has a refractive index of 1.385 [41] [42] [44] [45].

For each of these cell lines, we record the transmission spectrum. By filling the analyte inside the ring shaped cylinder, there is change in refractive index in the sensing region, giving a corresponding shift in the peak resonant wavelength. With an increase in RI value, the graph shifts towards right. As discussed above, the cancerous cell lines have higher RI values as compared to normal cell lines, so we observe a right shift in the graph. This property can be used to differentiate between the cell lines of a normal human being and those having cancer. Fig 26(a) shows the transmission spectra for basal cells, Fig 26(b) shows the transmission spectra for HeLa, and Fig 26(c) shows the result for MDA-MB-231.

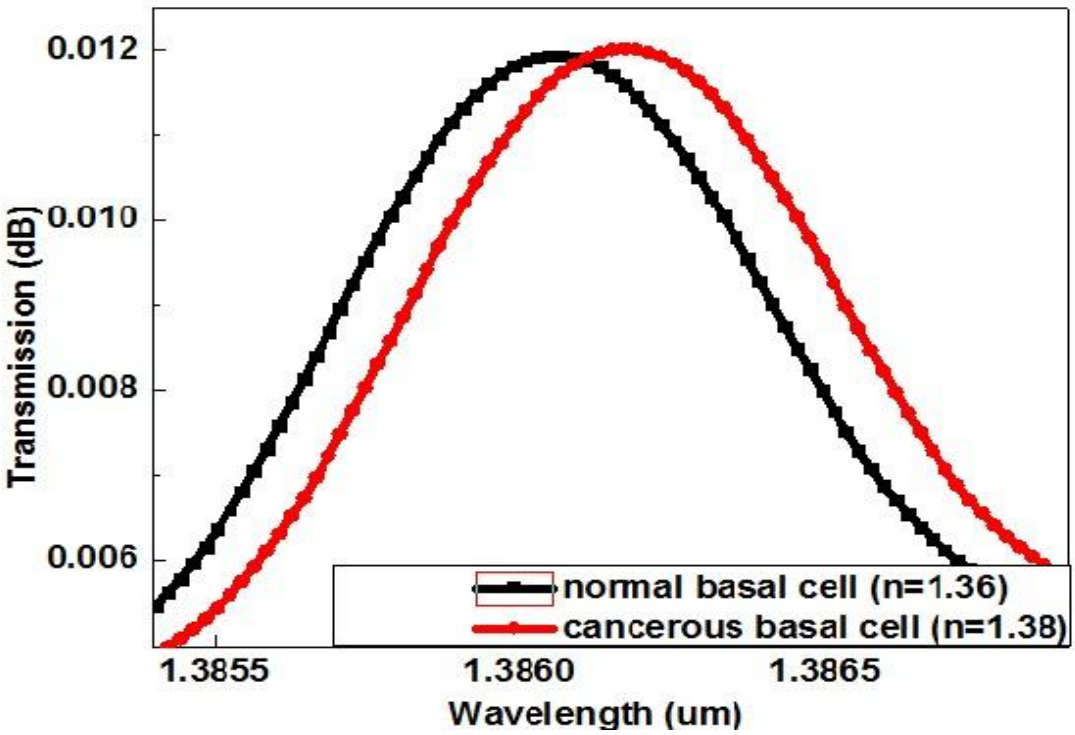

Fig 26(a) Output spectrum for Basal cancer cells

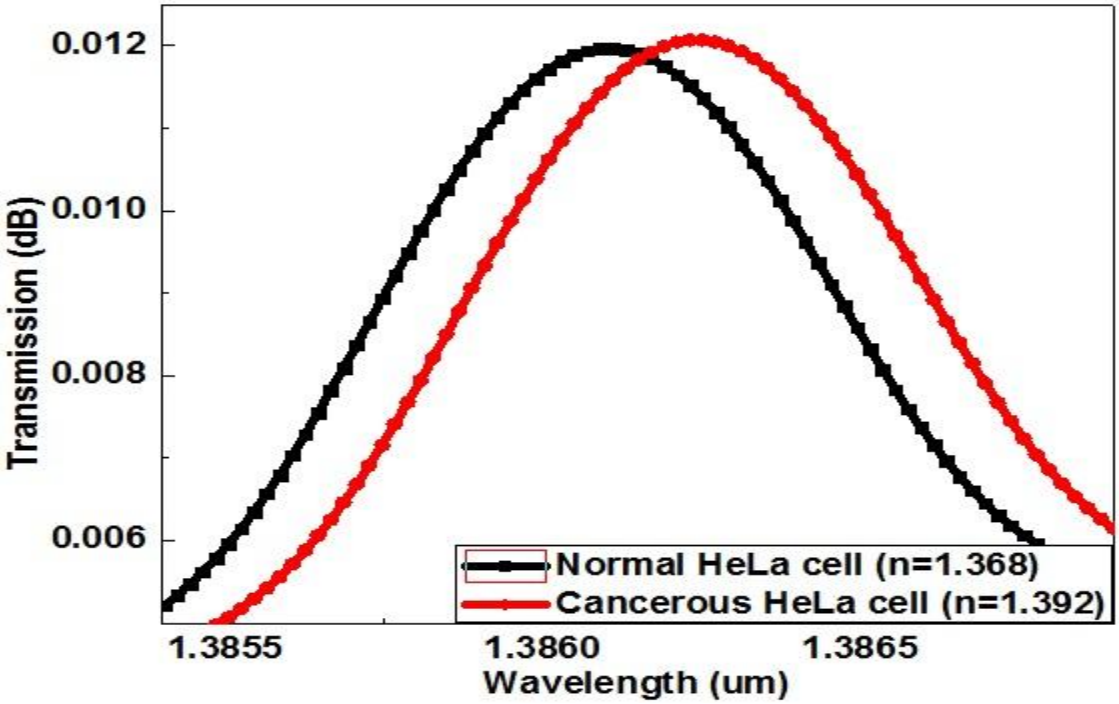

Fig 26(b) Output spectra for Hela cell lines

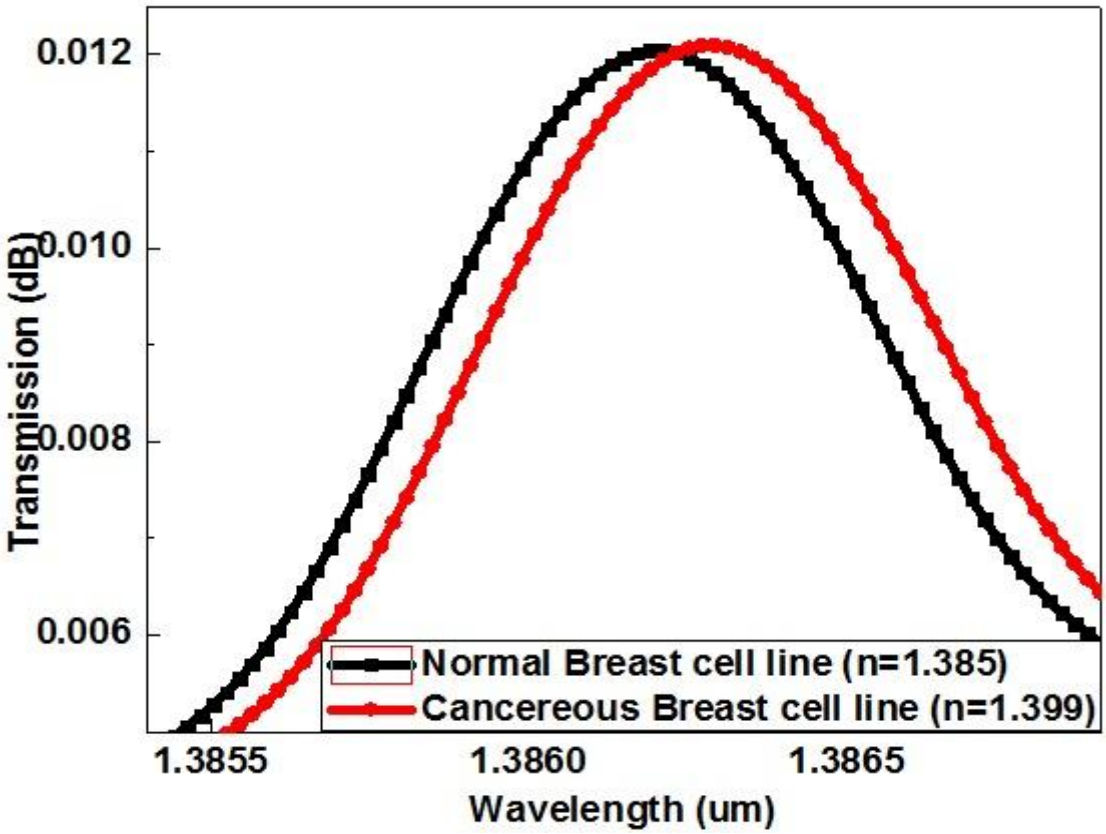

Fig 26(c) Output spectra for MDA-MB-231 cell line

Next, in order to detect whether a person has diabetes or not, samples of human tear are used. Again by using Atago's refractometer, refractive index value for normal cells (non-diabetic) is found to be equal to 1.35 and that of diabetic cells comes out to be 1.41. This process also works out by using water as the base analyte. By the principle explained above, diabetic cells have greater RI value, so we observe a right shift in the peak resonance wavelength as be seen in Fig 27.

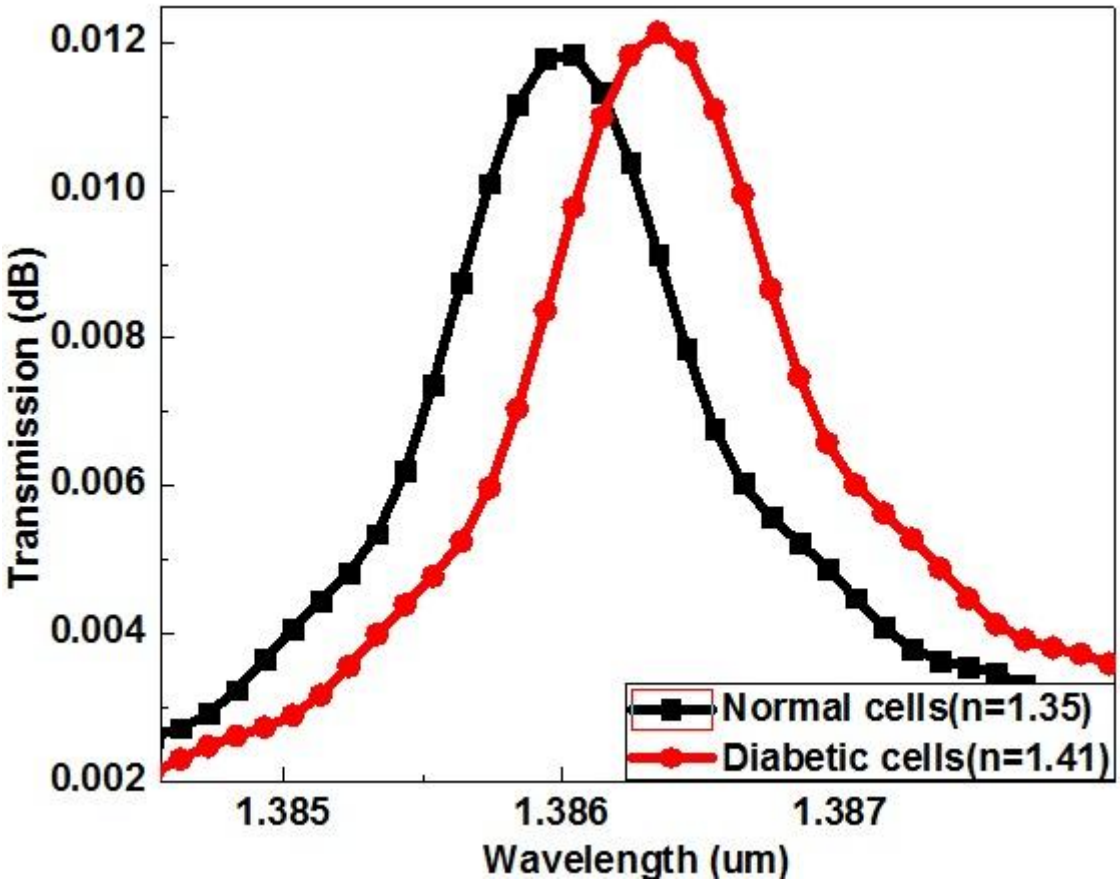

Fig 27 Output spectra as obtained by using human tear as an analyte

The quality factor (Q) is denoted by λmax/FWHM, where λmax is the peak resonant wavelength and FWHM denotes the full width half maximum value. Q value is recorded for each analyte and it is observed that with the increase in RI values or with the increase in peak resonant wavelength, quality factor decreases. The Q values along with the peak resonant wavelengths for each of the analytes are shown in Table 3. The sensitivity of a photonic crystal as discussed in the previous chapters, which expressed as the ratio of shift in peak resonant wavelength (Δλ) and the change in refractive index (Δn) of the analyte is also calculated in Table 3 below.

ANALYTE USED	REFRACTIVE INDEX	λmax	QUALITY FACTOR	SENSITIVITY
BASAL CELL (NORMAL)	1.36	1.38606367	1106.77	Ref
BASAL CELL (CANCEROUS)	1.38	1.38617672	1082.89	5.6525
HELA CELL (NORMAL)	1.368	1.38610384	1094.68	Ref
HELA CELL (CANCEROUS)	1.392	1.38625066	1090.82	6.5764
MDA-MB-231 CELL (NORMAL)	1.385	1.38619698	1094.76	Ref
MDA-MB-231 CELL (CANCEROUS)	1.399	1.38628905	1086.90	6.1175
NORMAL CELLS OF DIABETES	1.35	1.38602132	1100.81	Ref
EFFECTED CELLS OF DIABETES	1.41	1.38636073	1062.18	5.6568
WATER	1.33	1.38588	1110.48	Ref
BLOOD PLASMA	1.35	1.3860008	1084.16	5.3265
WBC'S	1.36	1.38605293	1078.47	5.28886
HAEMOGLOBIN	1.38	1.38615947	1076.65	5.304
RBC'S	1.40	1.3862932	1069.22	5.699
BIOTIN-STREPTAVIDIN	1.45	1.38660827	1040.37	5.95

Table 3: List of sensitivity and quality factor values for various analytes

CHAPTER 5

INTEGRATION OF GROUP III-V SEMICONDUCTOR MATERIALS IN SILICON WAVEGUIDES FOR SENSITIVITY AND QUALITY FACTOR MEASUREMENTS

Silicon based photonic circuits provide the advantage of large scale integration with electronic circuits and hence they are becoming very attractive in the field of nanotechnologies [47] [48] [49]. In order to route signals in a chip over distances in the mm range with very low losses, silicon based crystals can be used. Silicon-on-Insulator (SOI) structures combine the benefits of high refractive index of silicon (RI=3.45) with the low refractive index of its corresponding oxide, i.e. silicon oxide (RI=1.45) and hence are being used since many decades for efficient confinement of light [50] [51]. Some of the additional advantages of these silicon substrates include low cost, high reliability and high quality [52]. Hence, by using this common substrate, high quality optical and mechanical devices can be produced. Silicon has an indirect band gap of 1.1.eV [53], hence silicon waveguides can only operate at wavelengths above 1100nm [54]. Because of this, in silicon based waveguides, shorter wavelength based lasers [55] and photo-detectors that work in longer wavelength ranges cannot be used [56]. Also, active functionalities such as light emission and second harmonic generation cannot be performed in these waveguides [54].

For achieving better properties, silicon based waveguides are integrated with group III-V semiconductors such as Aluminium Nitride (AlN), Indium Phospide (InP), Indium Nitride (InN) and hence can be utilized in the field of optoelectronic systems. Thus, silicon or silicon-on-insulator based devices are used for performing passive functions [57] [58] [59].

In order to perform active functionalities which are absent in silicon waveguides, Group III-V semiconductor materials can be used [60]. Group III-Nitrides are known for their exceptional wide band gap property and have been studied widely for various optoelectronic and photonics applications [61]. They are accompanied with high drift velocities, high mobility, high thermal conductivity, and better stability [62]. AlN is known for its low loss, provides better light guiding and is used to realize high quality optoelectronic devices [56]. It has the largest band gap among all the Group III-nitrides. AlN can be used to achieve efficient second harmonic generation because of its compatibility with silicon as a substrate [63] [64] [65].

InN, known for its interesting electronic properties has the lowest band gap and lowest effective mass among the Group III-nitrides [66]. InN is used as a thin film for the growth of gallium nitride over sapphire, by acting as a buffer layer because of its soft nature and low decomposition temperature [67]. Silicon is considered be the best substrate for InN as reported in previous studies, with a lattice mismatch of 7.9% [68].

For a light source at 1550nm wavelength, InP based PC's seem to be the most suitable choice. In order to realize both active and passive functionalities, such photonic devices can be used. They provide better thermal dissipation as compared to other group III-V semiconductor materials when it comes to performance [69]. InP based photonic crystals are known for their integration with conventional optoelectronic components on InP substrates [69].

In this chapter, four different types of PCW designs based on silicon only and integration of semiconductor materials with silicon have been proposed. Type-1 consists of three layers of silicon in which holes are etched up to the bottommost layer. Type-2, Type-3 and Type-4 consists of two AlN layers, InN layers and InP layers respectively with silicon slab sandwiched in between having the same thickness as that of semiconductor layers. As discussed below, these designs are studied for input light given at different slabs. The effect of direction of light propagation is studied for each of these semiconductor materials and results are compared with that of silicon only configuration (Type-1). Initially, the holes are filled with water and then the refractive index values are varied.

The principle used in measurement of sensitivity is same in previous chapters based on the shift in peak wavelength obtained by the change in refractive index values inside the crystal. Based on these results, the most suitable semiconductor material which can be used in integration with silicon and can be exploited in the field of nanofabrication and optoelectronic technologies is found here.

5.1 DESIGN AND ANALYSIS OF VARIOUS CONFIGURATIONS

The design here consists of 12 ×12 hexagonal geometry of holes in different configurations as discussed below. The holes are filled with water (RI=1.33). Radius of holes is taken to be 120 nm and the lattice constant is equal to 0.4 μm. Finite difference time domain (FDTD) algorithm explained above as obtained by solving time dependent Maxwell's equations is used here [29].

Plane wave expansion (PWE) method is used to solve the band structure. By launching a temporal light pulse into the waveguide, photonic band gap (PBG) is obtained without introducing any defects in the waveguide. PBG exists for transverse magnetic (TM) mode and extends from 0.520096-0.650737 (1/λ). The corresponding wavelength obtained lies between 1536.71 nm-1922.72 nm. Hence, 1550 nm is considered as the central wavelength. By removing holes from the centre, defects are introduced in the crystal as shown below. For obtaining the output transmission spectrum, time monitor is used.

Four types of PCW designs are discussed and studied. In Type-1 configuration, three slabs of silicon each with a thickness equal to 500 nm and holes etched up to the bottommost slab are taken. The integration of silicon with different Group III-V semiconductor materials is shown in Type-2, Type-3 and Type-4 configuration with each layer having a thickness of 500 nm. In Type-2 configuration, silicon slab is sandwiched between two AlN layers. Type-3 shows silicon slab sandwiched between two InN layers and Type-4 shows silicon sandwiched between two InP layers. Fig 28(a)-(d) shows the various configurations as discussed above. Various directions are also shown for the waveguide when placed in x-z orientation.

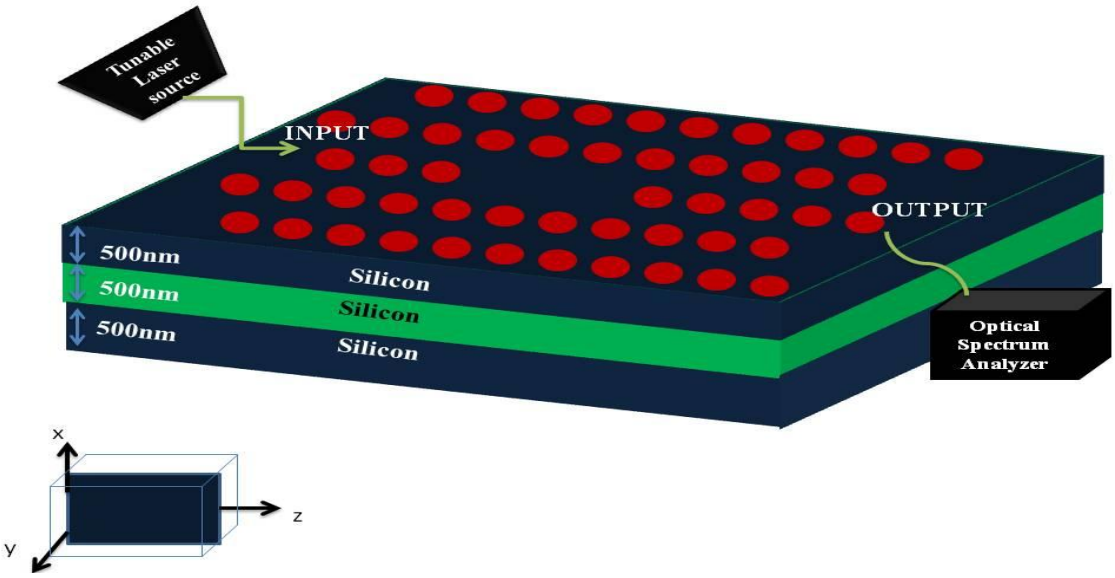

Fig 28(a) Type-1 configuration showing silicon based photonic crystal waveguide.

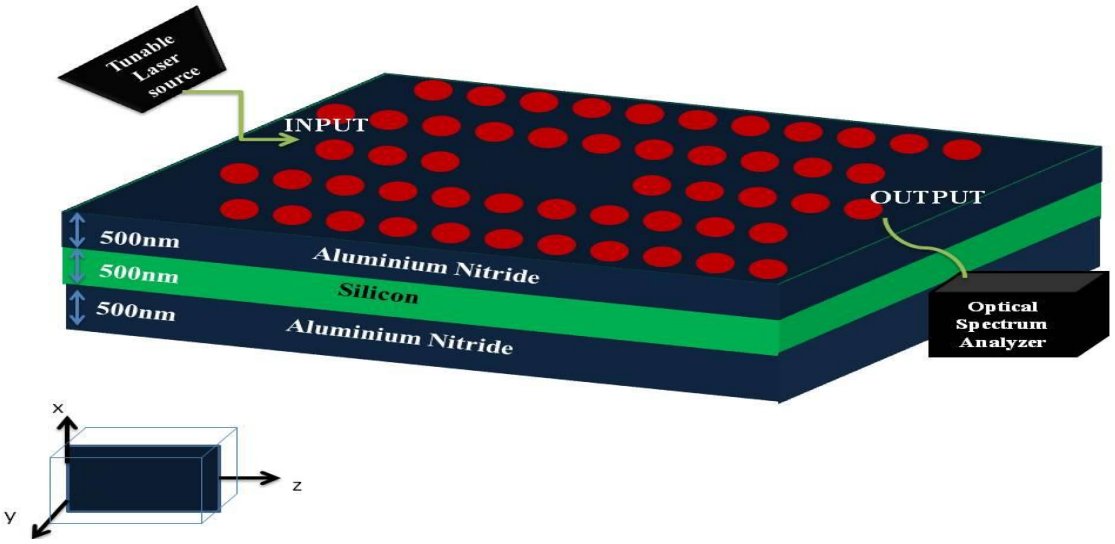

Fig 28(b) Type-2 configuration showing silicon and aluminium nitride based photonic crystal waveguide.

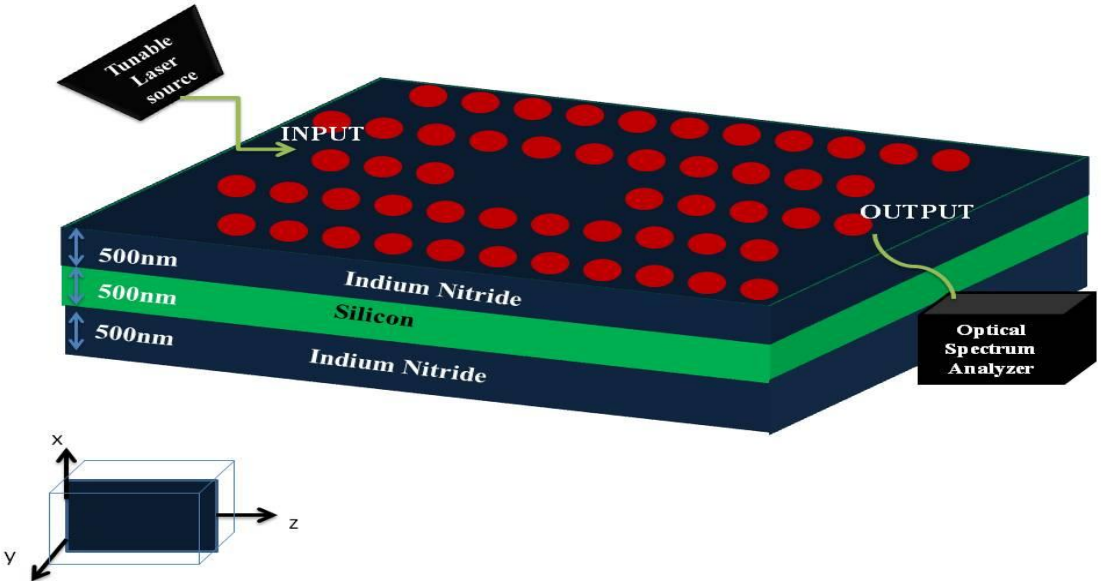

Fig 28(c) Type-3 configuration showing silicon and indium nitride based photonic crystal waveguide.

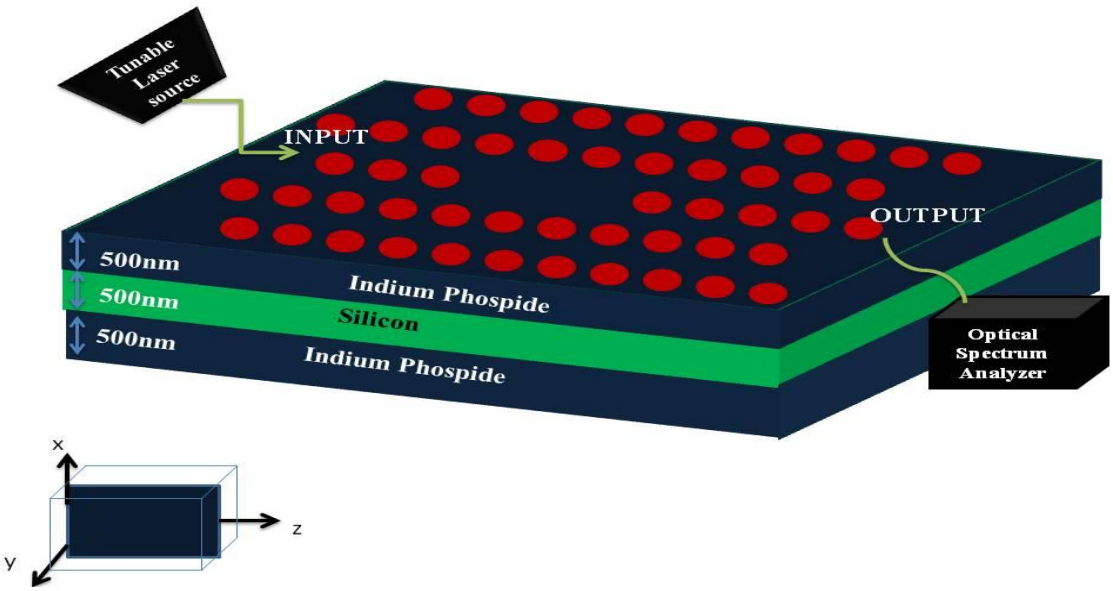

Fig 28(d) Type-4 configuration showing silicon and indium phospide based photonic crystal waveguide.

5.2 EFFECT OF INPUT LAUNCHED AT DIFFERENT POSITIONS

We consider that the light is launched at positions y=0.25, y=0.75 and y=1.25 in order to take into account the effect of each slab for each of the above configurations. For different positions of light propagation through the waveguide, transmission spectrum is recorded. Because of the difference among refractive indices of different slabs, the process of total internal reflection occurs which leads to trapping of light inside the waveguide in the vertical direction. We observe that, there is an increase in guiding mode energy as the light travels inside the waveguide since the holes are etched up to the bottommost slab, giving rise to an increase in the transmission strength. As the input light moves from position y=1.25 towards y=0.25 inside the slab, there is a right shift in the peak wavelength. Hence the sensitivity value increases. Fig 29 and 30 represent the transmission vs. wavelength spectrum for Type-3 and Type-4 configuration. Fig 31 shows the transmission spectra for Type-1 (PCW based on silicon only configuration). Fig 32 shows that as the light travels inside the waveguide, there is a decrease in transmission spectra as observed only for Type-2 configuration that is based on integration of AlN with silicon. The curve depicted by square boxes corresponds to light entering the waveguide at the bottom most slab, i.e. y=0.25 and the curve depicted by triangular boxes shows the transmission for light entering the waveguide at position y=1.25. Transmission strength and hence the sensitivity decreases for AlN because of its low refractive index value (RI=2.12) as compared to silicon (RI=3.45), leading to a decrease in effective refractive index value.

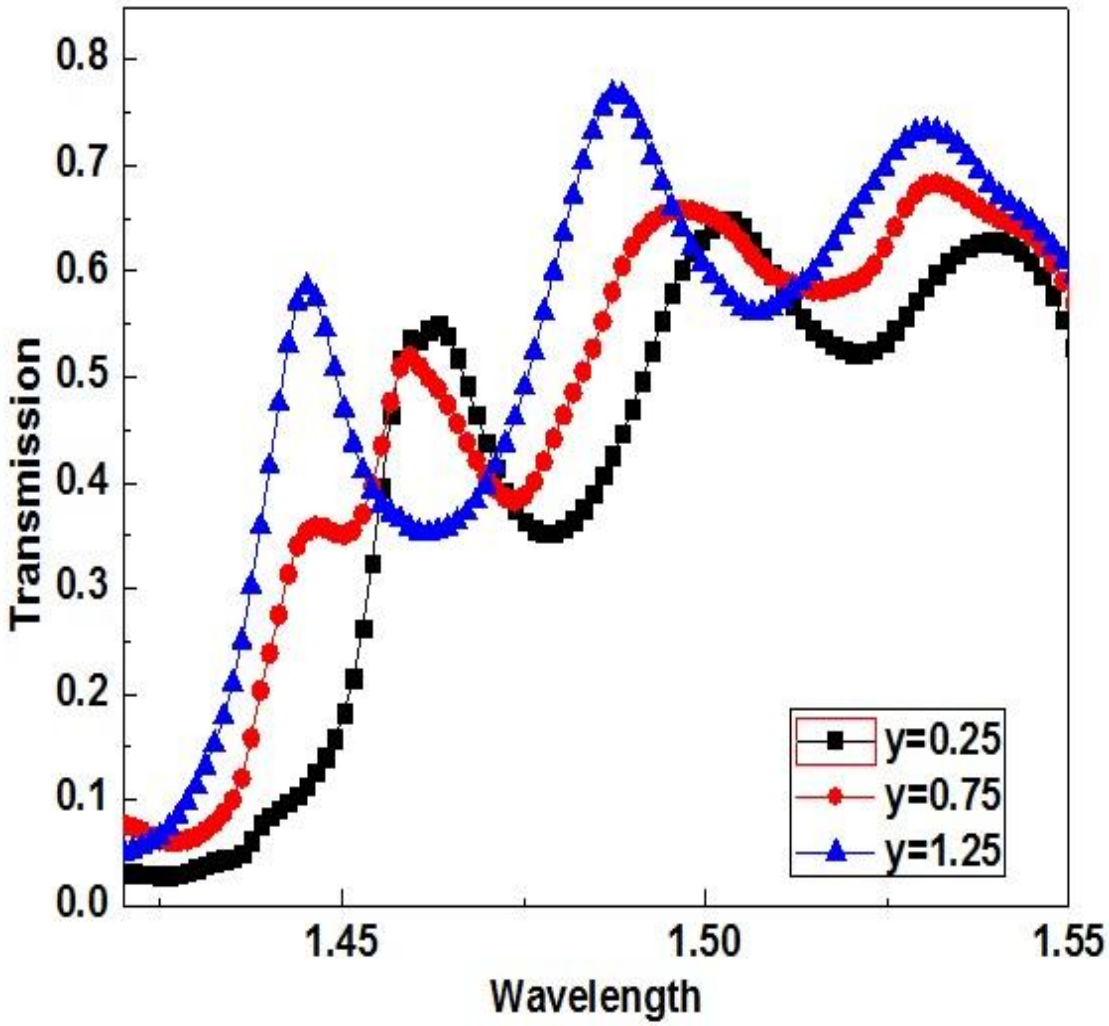

Fig 29 Transmission spectra for Type-3 configuration showing the effect of different positions at which input light is launched taking into account the different layers of the PCW.

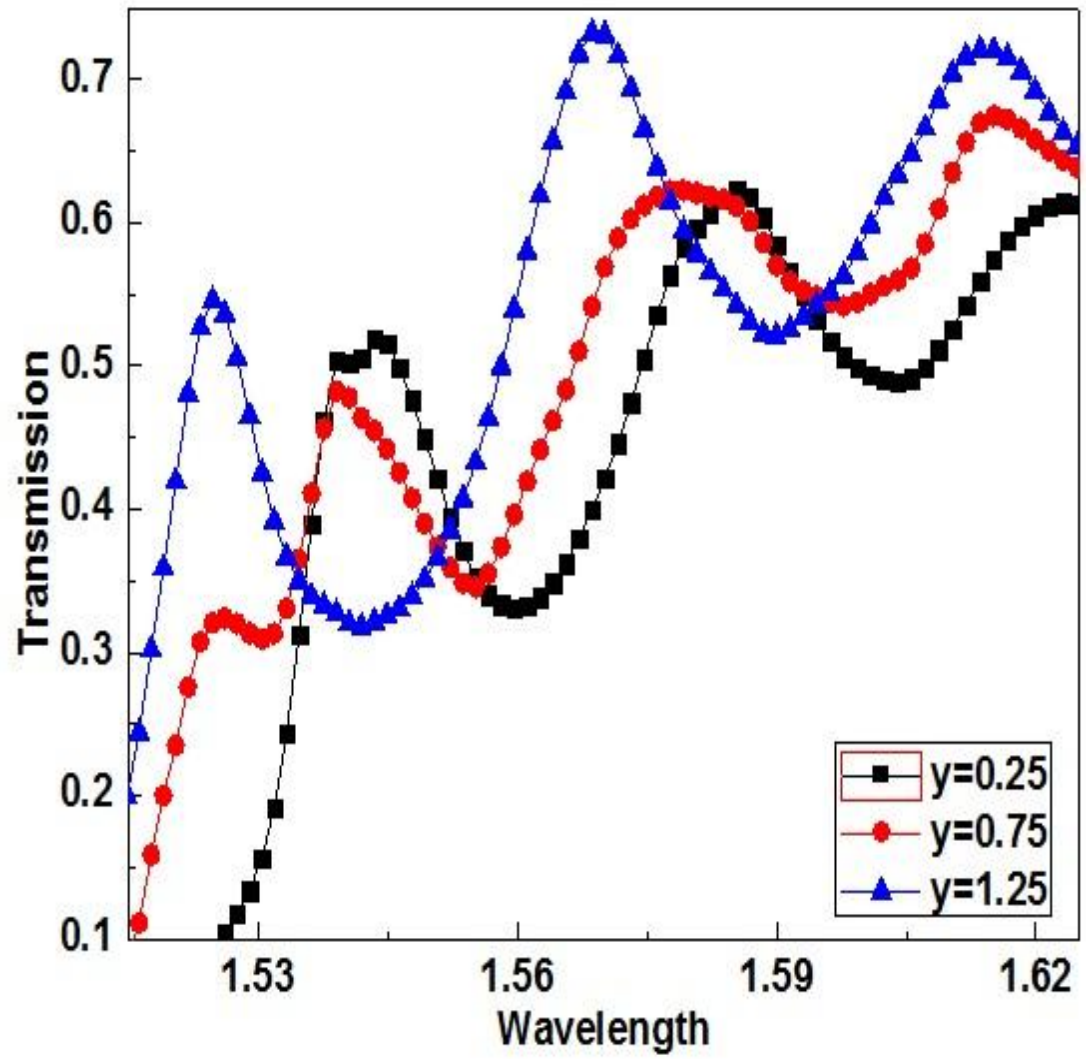

Fig 30 Transmission spectra for Type-4 configuration showing the effect of different positions at which input light is launched taking into account the different layers of the PCW.

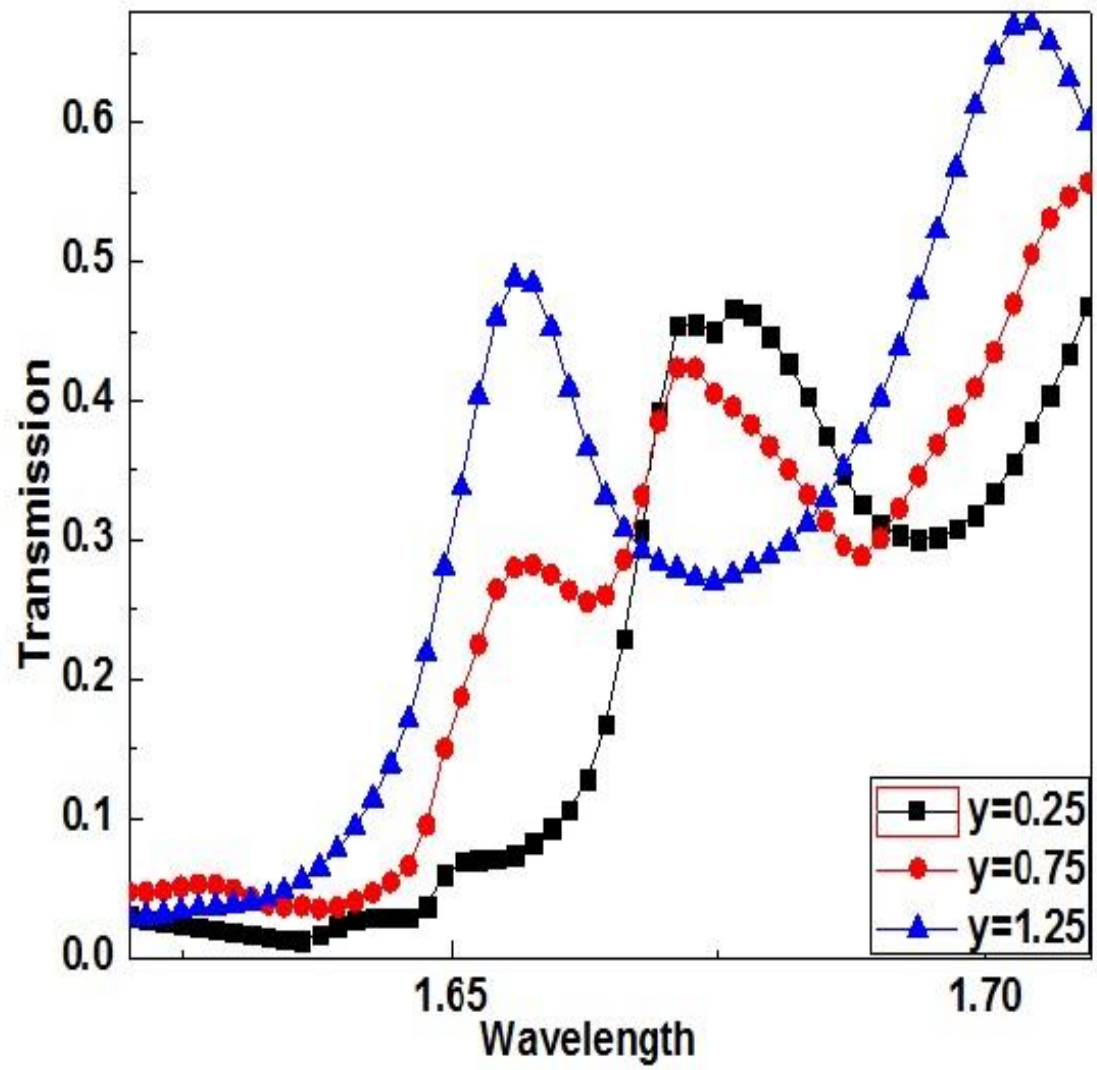

Fig 31 Transmission spectra for Type-1 configuration showing the effect of different positions at which input light is launched taking into account the different layers of the PCW.

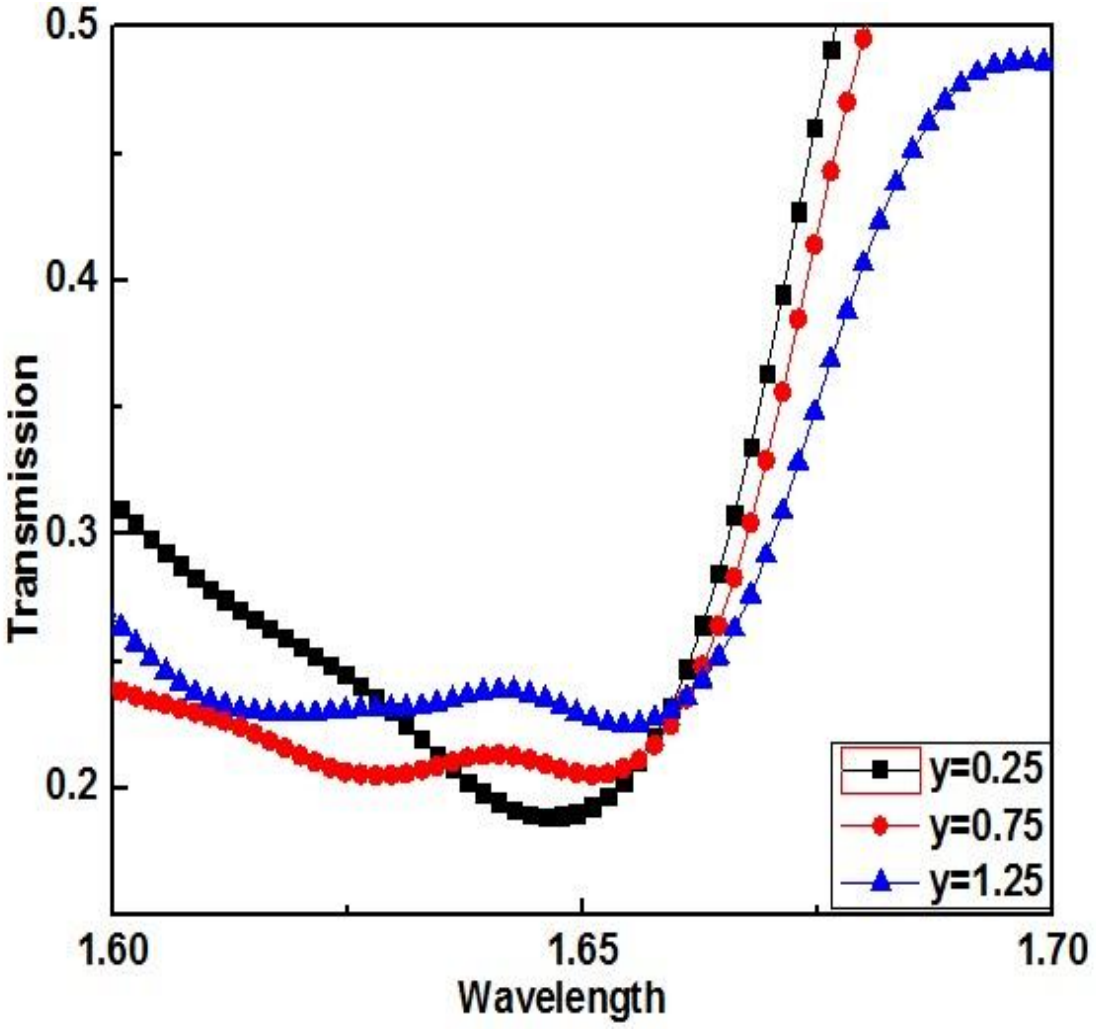

Fig 32 Transmission spectra for Type-2 configuration showing the effect of different positions at which input light is launched taking into account the different layers of the PCW

5.3 COMPARISON BETWEEN SILICON BASED AND SEMICONDUCTOR MATERIALS BASED PCW'S

In case of Type-2, 3 and 4, silicon core acts as the guiding layer with a higher refractive index. It is surrounded by two cladding layers which are made up of the semiconductor materials of lower refractive indices. In these three different layers, light propagates along the plane. Within the middle slab, it is confined by the process of index guiding. The effective refractive index or the modal refractive index comes into play due to difference between the refractive indices of the core and cladding

layers. It depends on the material that is used and takes into account the design as a whole.

In order to overcome the drawbacks that are faced by configurations such as silicon rods suspended in air, the above mentioned design of a higher index core surrounded by low index semiconductors plays an important role. Due to the low refractive index contrast, the mode starts penetrating into the respective cladding layers. Since the holes are etched up to the bottom most slab, this drawback is overcome in our design and hence a sufficient modal overlap is achieved. With the help of this etching, an ease of fabrication and better confinement of guided modes is achieved. By adding low index materials on both sides of the silicon slab, larger photonic band gap exists.

The transmission of light in Type-1 configuration is compared with that in other configurations to take into account the effect of using different semiconductor materials.

With the use of semiconductor materials, a right shift is obtained along with an increase in the overall intensity of light passing through the waveguide. Fig 33(a)-(c) shows the results of this comparison. Table 4 shows the peak wavelength values obtained for each configuration when compared with Type-1. A right shift of 164.9 nm, 83.61 nm, and 96.93 nm is obtained when Type-1 is compared with Type-2, 3 and 4 respectively.

Sensitivity of the device which is expressed as the ratio of change in peak wavelength ($\Delta\lambda$) by the change in refractive index (Δn) is calculated for each case as shown in Table 4. From the calculated values, maximum shift in peak resonant wavelength is observed for the case of Indium Phospide based PCW giving a sensitivity value of 346.9 nm/RIU.

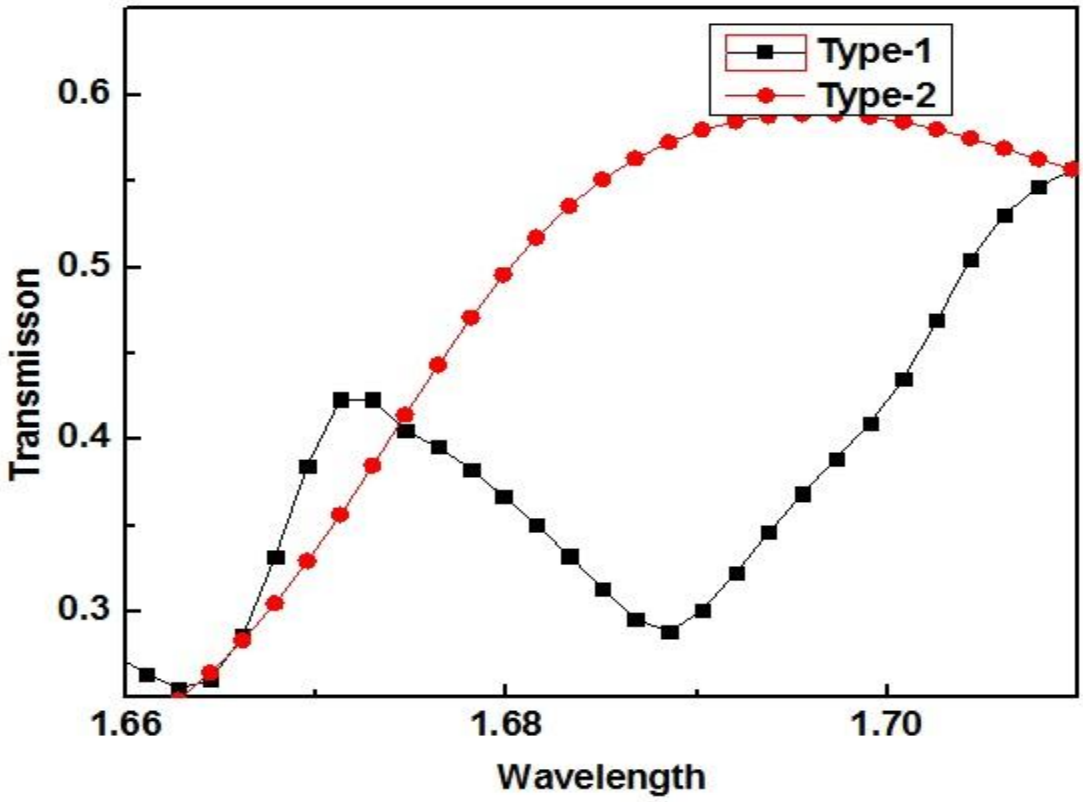

Fig 33(a) Transmission spectra for Type-1 and Type-2 configuration

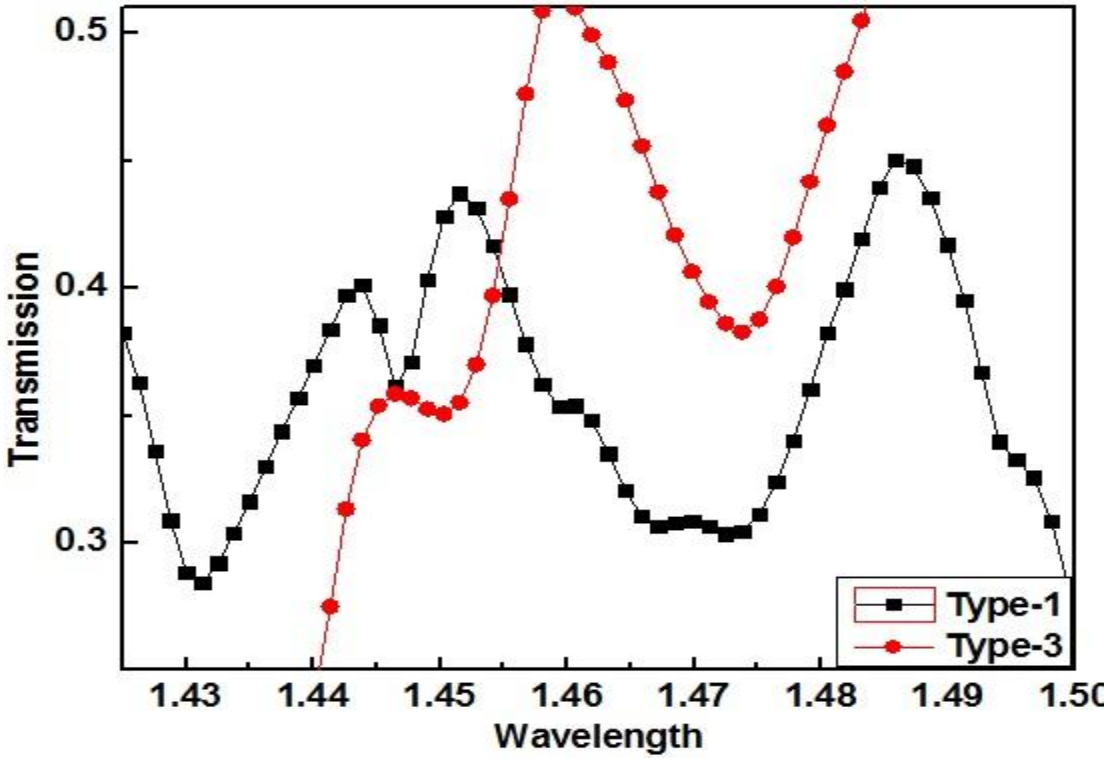

Fig 33(b) Transmission spectra for Type-1 and Type-3 configuration

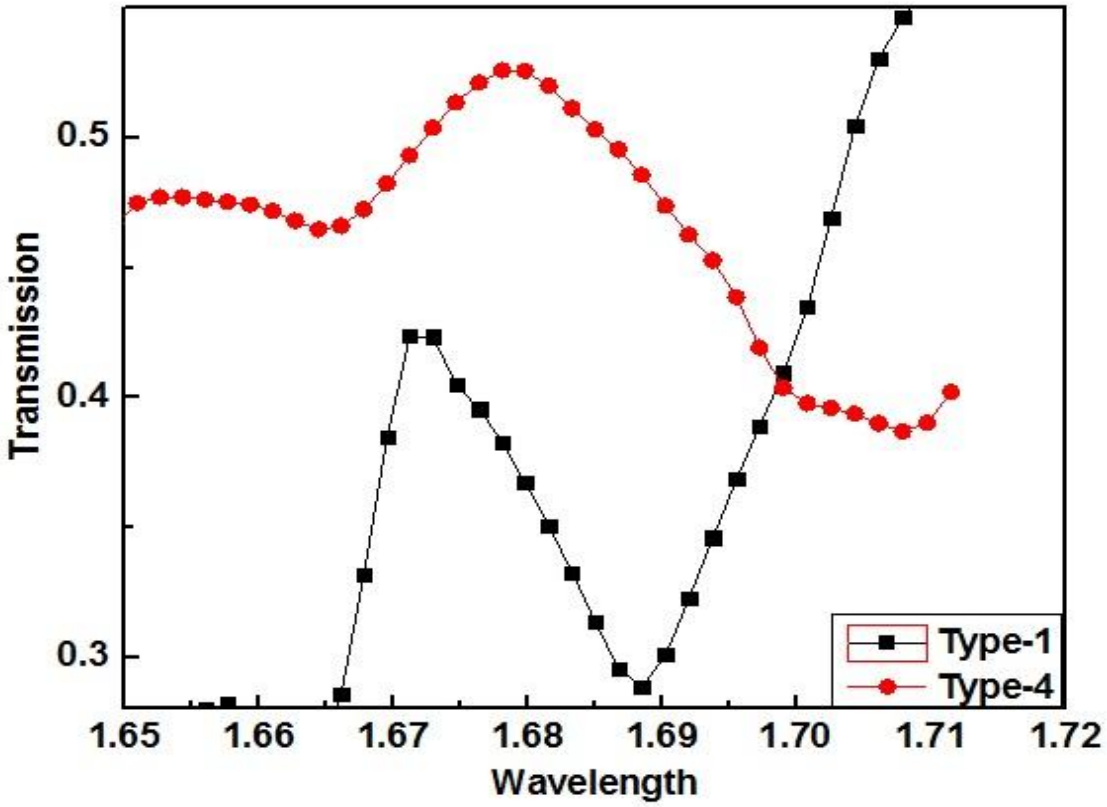

Fig 33(c) Transmission spectra for Type-1 and Type-4 configuration

DESIGN TYPE	Δλ (SHIFT IN PEAK WAVELENGTH) measured in nm	Δn (CHANGE IN REFRACTIVE INDEX)	SENSITIVITY (nm/RIU)
Type-1	424.42		
Type-2	589.34	1.33	123.9
Type-1	436.39		
Type-3	520	0.45	185.7
Type-1	289.29		
Type-4	386.22	0.28	346.19

Table 4: List of sensitivity values as obtained for the various configurations taking type-1 as the reference

5.4 SENSITIVITY MEASUREMENT BASED ON CHANGE IN RI VALUES

Initially, for this structure the holes are filled with water (RI=1.33). A shift in the peak wavelength is obtained when we change the refractive index of holes to a higher value. Hence, an increase in sensitivity is observed. The refractive index of hole is then changed from 1.33 to 1.45. The peak resonant wavelengths are recorded and sensitivity values are calculated for each configuration. Table 5(a)-(d) shows the sensitivity values for each configuration.

REFRACTIVE INDEX OF THE ANALYTE USED FOR HOLES (n)	**PEAK WAVELEN-GTH measured in nm**	**Δλ (SHIFT IN PEAK WAVEL-ENGTH) measured in nm**	**Δn (CHANGE IN REFRACTI-VE INDEX)**	**SENSITIVI-TY (nm/RIU)**
1.33	397.978			
1.38	418.956	20.978	0.05	419.55
1.41	484.102	86.124	0.08	1076.66
1.45	496.476	98.498	0.12	820.81

Table 5(a) List of sensitivity values obtained by changing the refractive index of holes for type-1 configuration

REFRACTIVE INDEX OF THE ANALYTE USED FOR HOLES (n)	**PEAK WAVELEN-GTH measured in nm**	**Δλ (SHIFT IN PEAK WAVEL-ENGTH) measured in nm**	**Δn (CHANGE IN REFRACTI-VE INDEX)**	**SENSITIVI-TY (nm/RIU)**
1.33	494.345			
1.38	512.851	18.506	0.05	370.12
1.41	525.757	31.412	0.08	392.65
1.45	543.444	49.099	0.12	409.15

Table 5(b) List of sensitivity values obtained by changing the refractive index of holes for type-2 configuration

REFRACTIVE INDEX OF THE ANALYTE USED FOR HOLES (n)	PEAK WAVELEN-GTH measured in nm	Δλ (SHIFT IN PEAK WAVEL-ENGTH) measured in nm	Δn (CHANGE IN REFRACTI-VE INDEX)	SENSITIVI-TY (nm/RIU)
1.33	649.407			
1.38	656.864	7.457	0.05	149.13
1.41	661.720	12.313	0.08	153.9
1.45	668.107	18.7	0.12	155.8

Table 5(c) List of sensitivity values obtained by changing the refractive index of holes for type-3 configuration

REFRACTIVE INDEX OF THE ANALYTE USED FOR HOLES (n)	PEAK WAVELEN-GTH measured in nm	Δλ (SHIFT IN PEAK WAVEL-ENGTH) measured in nm	Δn (CHANGE IN REFRACTI-VE INDEX)	SENSITIVI-TY (nm/RIU)
1.33	455.258			
1.38	464.545	9.287	0.05	185.7
1.41	472.302	17.044	0.08	213
1.45	480.060	24.802	0.12	206.6

Table 5(d) List of sensitivity values obtained by changing the refractive index of holes for type-4 configuration

Maximum sensitivity of 1076.66nm/RIU is observed for Type-1 configuration when refractive index of holes is equal to 1.41. In case of Group III-V semiconductor materials, maximum sensitivity is observed in case of Type-2 configuration with an average sensitivity value of 390.64 nm/RIU. For Type-3 and Type-4 configuration, average sensitivity value of 152.94nm/RIU and 201.76nm/RIU is obtained respectively.

CHAPTER 6

CONCLUSION AND FUTURE WORK

6.1 CONCLUSION

The entire work has been focused in designing sensors based on photonic crystal waveguides using different hole shapes, various etch depths, using different semiconductor layers, introducing cavities, by introducing light at different positions inside the crystal to observe the enhancement in sensitivity as obtained by change in RI values inside the crystal.

The work focuses on three areas- (a) gas sensor designed using ring shaped holes; (b) a bio-sensor designed for detection of diseases and (c) integration of suitable semiconductor layer with silicon for best sensitivity results using best semiconductor materials.

In the **first part**, a gas based sensor using ring shaped holes is considered. The input wavelength is taken as 1.45μm. After introducing the line defect, transmission spectra was obtained for different holes diameters and it was found that transmission cannot be analyzed beyond holes diameter of 0.27 μm because the range of forbidden band gap increases converting guided modes into leaky modes. Also, with the increase in defect holes diameter, the sensitivity increases.

Further enhancement in sensitivity was measured by etching in silicon guiding layer and up to a certain depth in the buried oxide layer. It was observed that the sensitivity increases up to an etch depth of 0.04 μm after which it is found to be decreasing.

After this, infiltration with different gaseous analytes was done to measure the sensitivity based on the shift in the cut off wavelength as observed because of the change in refractive index of the structure. Sensitivity of 675nm/RIU is obtained. Hence this sensor can be used to sense different gases like hydrogen, ammonia, nitrogen etc. These gases have refractive indices values close to that of air.

In the **second part**, we have presented a bio-sensor based on photonic crystal waveguide with ring resonator which can be used for the detection of diseases. The input wavelength is taken as 1550nm. By binding the analyte into the sensing region, transmission spectrum is recorded. The sensing mechanism of the bio-sensor is based on shift in peak resonant wavelength obtained by the change in refractive index. The transmission spectrum shifts towards right for greater RI values. Quality factor and sensitivity values are calculated for the same. It is observed that as the refractive index of the analyte increases, Q value decreases. Average value of quality factor for this device comes out to be 1082.2. Sensitivity values increases with the increase in RI values. For 0.02 change in RI, sensitivity increases by 0.0154nm/RIU.

In the **third part**, a 3D photonic crystal waveguide is designed based on four different configurations. Conventional PCW's are based on holes in a silicon background. We studied the effects of integrating Group III-V semiconductor materials such as AlN, InN, InP with silicon slab. The silicon slab which forms the core is surrounded by these materials on both sides maintaining the symmetry. The holes are etched up to the bottom most slab for effective confinement of light through the crystal. Firstly, by taking into account each layer, the light is launched at different positions for each configuration. There is decrease in transmission strength as light moves inside the crystal for the case of AlN, due to decrease in effective refractive index. Secondly, Type-1 configuration is compared with all other configurations to study the effect of semiconductor materials used. Maximum sensitivity of 346.19 nm/RIU is obtained for Type-4 configuration based on InP. Lastly, the refractive index of the holes which is initially taken as 1.33 is changed to higher values. A shift in peak wavelength is obtained with this change. Maximum sensitivity is obtained for silicon based PCW and for AlN in case of semiconductor material based PCW. But due to the decrease in transmission strength as explained above AlN does not seems to be a suitable choice. Taking into consideration all of the above factors, InP seems to be an appropriate material for integration with silicon. The transmission strength increases as light moves deep inside the crystal and highest sensitivity is obtained for InP based PCW when compared with silicon based PCW as explained above.

6.2 FUTURE SCOPE

1. This work can be further optimized by using different hole shapes such as elliptical shaped or a ring with the outer hole elliptical in shape and the inner hole circularly shaped.
2. Different sensing areas can be taken inside a single crystal to observe simultaneous interaction of analyte with the receptors in an aqueous environment.
3. Further, 1D crystals can be designed and fabricated which obviously leads to a less complex structure.
4. Other parameters such as figure of merit or selectivity can also be achieved which has not been discussed in the present work.

REFERENCES

[1] C. Jamois, R. B. Wehrspohn, L.C. Andreani, C. Hermann, O. Hess , and U. Gösele, "Silicon-based two-dimensional photonic crystal waveguides," *Photonics and Nanostructures – Fundamentals and Applications*, vol. 1, pp.1–13, 2003.

[2] Y. Zhao, Y. N. Zhang, Q. Wang, and H. Hu, "Review on the Optimization Methods of Slow Light in Photonic Crystal Waveguide," *IEEE Transactions on Nanotechnology*, vol. 14, pp. 407-426, 2015.

[3] A.K. Goyal and S. Pal, "Design and simulation of high-sensitive gas sensor using a ring-shaped photonic crystal waveguide," *Royal Swedish Academy of Sciences*, pp. 1-5, 2015.

[4] A.K. Goyal and S. Pal, "Design and simulation of high sensitive photonic crystal waveguide sensor," *Optik 126*, pp. 240–243, 2015.

[5] H. Dutta, A.K. Goyal, and S. Pal, "Sensitivity enhancement in photonic crystal waveguide platform for refractive index sensing applications," *J. Nanophoton*, vol. 8, pp. 1-7, 2014.

[6] F. Bagci and B. Akaoglu, "Enhancement of Refractive Index Sensitivity in Photonic Crystal Waveguide-Based Sensors by Selective Infiltration," *APhysPolA*, vol. 124, pp. 50-55, 2013.

[7] F. Bougriou, T. Boumaza, M. Bouchemat, and N. Paraire, "Sensitivity analysis of a photonic crystal waveguide for refraction index sensing," *Physica Scripta*, pp. 1-4, 2012.

[8] M. Doss, M. Subadra, "3D design and computation of ring resonator with nano photonic crystal using FDTD modelling," *AIP Conf. Proc*., vol. 1391, pp. 257-259, 2011.

[9] M. Pu, L. Liu, L.H. Frandsen, H. Ou, K. Yvind, and J.M. Hvam, "Silicon-on-insulator ring-shaped photonic crystal waveguides for refractive index sensing," *Proc. of Conf. on OFC/NFOEC*, pp. 1–3, 2010.

[10] T. Sünner, T. Stichel, S.H. Kwon, T.W. Schlereth, S. Höfling, M. Kamp, and A. Forchel, "Photonic crystal cavity based gas sensor," *Appl. Phy. Lett*, vol. 92, pp. 261112, 2008.

[11] X. Wang, N. Lu, J. Zhu, and G. Jin, "An ultra-compact refractive index based gas sensor based on photonic crystal micro-cavity," *Proc. SPIE*, vol. 6831, 2008.

[12] R. Hao, H. Kurt, D.S. Citrin, and Z. Zhou1, "The complete band gap in ring-shaped photonic crystal SOI slab," *Proc. Of IEEE Conf. on Group IV Photonics*, pp. 291–293, 2008.

[13] A. Saynatjoki, M. Mulot, K. Vynck, D. Cassagne, J. Ahopelto, and H. Lipsanen, "Properties, applications and fabrication of photonic crystals with ring-shaped holes in silicon-on-insulator," *Photonic Nanostruct*, vol. 6, pp. 42–46, 2008.

[14] T. Hasek, H. Kurt, D.S. Citrin, and M. Koch, "Photonic crystals for fluid sensing in the subterahertz range," *Appl. Phys. Lett.*, vol. 89, pp. 1-3, 2006

[15] H. Kurt and D.S. Citrin, "Annular photonic crystals", *Opt. Express*, vol. 13, pp. 10316–10326, 2005.

[16] D.E. Dood M J A, E. Snoeks, A. Morozand, and A. Polman,"Design and optimization of 2D-photonic crystal waveguide based on silicon," *Opt. Quant. Electron*, vol. 34, pp. 145–159,2002.

[17] B.J. Luff, R.D. Harris, and J.S. Wilkinson, "Integrated-optical directional coupler biosensor," *Opt. Lett.*, vol. 21, pp. 618-620, 1996.

[18] American Cancer Society. (2016). *Cancer Facts & Figs* [Online]. Available: http://www.cancer.org

[19] Cancer Research UK. (2015). *Bowel cancer survival statistics* [Online]. Available: http://www.cancerresearchuk.org/about-cancer/cancer symptoms/why-is-early-diagnosis-important.

[20] S.R Joshi, A.K. Das, V.J. Vijay, and V. Mohan, "Challenges in diabetes care in India: Sheer numbers, lack of awareness and inadequate control," in *J Assoc Physicians India*, 2008, pp. 443–50.

[21] J Nissl. (2009, September). *Complete blood count* [Online]. Available: http://www.webmd.com/a-to-z-guides/complete-blood-count-cbc

[22] Rowan University. (2015, October). *Blood-based biomarkers for early detection, diagnosis and staging of Parkinson's disease* [Online]. Available: www.sciencedaily.com.

[23] Poonam Sharma et al., "A Photonic Crystal sensor for Analysis and Detection of Cancer cells," in *2015 International Conference on Pervasive Computing (ICPC)*, pp. 1 – 5.

[24] J. Zhang, W. Hodge, C. Hutnick, and X. Wang, "Non invasive Diagnostic Devices for Diabetes through Measuring Tear Glucose," *J. Diabetes Sci. Technol.*, vol. 5, pp. 166–172, 2011.

[25] P. Makaram, D. Owens, and J. Aceros, "Trends in Nanomaterial-Based Non-invasive Diabetes Sensing Technologies," *Diagnostics*, vol. 4, pp. 27-46, 2014.

[26] Q. Yan, B. Peng, G. Su, B. E. Cohan, T. C. Major, and M. E. Meyerhoff, "Measurement of Tear Glucose Levels with Amperometric Glucose Biosensor/Capillary Tube Configuration," *Anal. Chem.*, vol. 83, pp. 8341–8346, 2011.

[27] S. Olyaee and A. Naraghi," Design and optimization of index guiding photonic crystal fiber gas sensor," *Photonic Sens.*, vol.3, Issue 2, pp. 131–136, 2013.

[28] Y. Sugimoto, Y. Tanaka, N. Ikeda, T. Yang, H. Nakamura, K. Asakawa, K. Inoue, T. Maruyama, K. Miyashita, K. Ishida, and Y. Watanabe, "Design, fabrication, and characterization of coupling-strength controlled directional coupler based on two-dimensional photonic-crystal slab waveguides," *Appl. Phys. Lett.*, vol.83, pp. 3236–3238, 2003.

[29] S. Chakravart, Y. Zou, W. Lai, and R. Chen,"Slow light engineering for high Q high sensitivity photonic crystal microcavity biosensors in silicon," *Biosens. Bioelectron*, vol. 38, Issue 1, pp. 170–176, June 2012.

[30] The Science Company. (2016). *Refractometers* [Online]. Available: http://www.sciencecompany.com/Atago-Digital-Refractometer-PAL-RI-13306-15284-P16382.aspx.

[31] A. N. Shvalov, J.T. Soini, A. V. Chernyshev, P. A. Tarasov, E. Soini, and V. P. Maltsev, "Light-scattering properties of individual erythrocytes," *Appl. Optics*, vol. 38, pp. 230-235, January 1999.

[32] J. Mroczka and D. Wysoczanski, "Optical parameters and scattering properties of red blood cells," *Optica Applicata*, vol. 32, Issue no. 4, pp. 691-700, 2002.

[33] X. Xu, R. K. Wang, J. B. Elder, and V. V. Tuchin, "Effect of dextran-induced changes in refractive index and aggregation on optical properties of whole blood," *Phys. Med. Biol*., vol. 48, pp. 1205-1221, May 2003.

[34] R.I. Ritter and S. Nandi, "Density Gradient Centrifugation of Red Blood cells carrying the Mammary Tumour Virus," *Nature*, vol. 220, pp. 403 – 404, October 1968.

[35] E. P. Diamandis and T. K Christopoulos, "The biotin-(strept)avidin system: principles and applications in biotechnology," *Clinical Chemistry*, vol. 37, Issue no. 5, pp. 625-636, May 1991.

[36] M. Friebel and M. Meinke, "Determination of the complex refractive index of highly concentrated hemoglobin solutions using transmittance and reflectance measurements," *J. Biomed. Opt*., vol. 10, Issue no. 6, 064019, 2005.

[37] H. C. Beck, M Overgaard, and L. M. Rasmussen, "Plasma proteomics to identify biomarkers – application to cardiovascular diseases," *Translational Proteomics*, vol. 7, pp. 40-48, June 2015.

[38] A. Zhbanov and S. Yang, " Microfluidic Blood Seperations through optical Sorting and Deterministic Lateral Displacement," in *ICQNM 2011 : The Fifth International Conference on Quantum, Nano and Micro Technologies*, pp. 103-108.

[39] Riley Hospital for Children. (2016). *White Blood Cell Disorder* [Online]. Available: http://iuhealth.org/riley/cancer/conditions-treated/white-cell-function-disorders.

[40] D. J. Wolf and J. A. Zitelli, "Surgical Margins for Basal Cell Carcinoma," Arch *Dermatol.*, vol. 123, Issue no. 3, pp. 340-344, 1987.

[41] R. Patel , A. N. Yaroslavsky, Lin, M. Al-Arashi, E. Salomatina, C. Li, C., and V. Neel, "High contrast mapping of basal cell carcinomas," *Opt. Lett.*, vol. 37, pp. 644-646, 2012.

[42] A.Q. Liu, X. Liang, P. Yap, X. M. Zhang, H. S. Yoon and T. C. Ayi, "Determination of refractive index for single living cell using integrated biochip," *Solid-State Sensors, Actuators and Microsystems*, vol. 2, pp. 1712 – 1715, 2005.

[43] Big Pictures. (2015). *Quick guide to HeLa cells* [Online]. Available: http://bigpictureeducation.com/quick-guide-hela-cells.

[44] P. Sharan, S.M. Bharadwaj, F.D. Gudagunti, and P. Deshmukh,"Design and modelling of photonic sensor for cancer cell detection," in *International conference on the Impact of E-Technology on US (IMPETUS), Bangalore*, Jan.10-11, 2014, pp.20-24.

[45] Elizabeth A. Thomson. (2001, January). *MIT News* [Online]. Available: http://news.mit.edu/2001/fenn-0110.

[46] R. Cailleau, R. Young, M. Olive and W. J. Reeves Jr.," Breast Tumor Cell Lines from Pleural Effusions," *J. Natl. Cancer Inst.*, vol. 53, pp. 661-674, 1974.

[47] R. Kirchain and L. Kimerling, "A roadmap for nanophotonics," *Nat Photonics*, vol. 1, pp. 303-305, 2007.

[48] B. Jalali and S. Fathpour, "Silicon Photonics," *J Lightwave Technol*, vol. 24, pp. 4600-4615, 2006

[49] W. Bogaerts, R. Baets, P. Dumon, V. Wiaux, S. Beckx, D. Taillaert, B. Luyssaert, J. V. Campenhout, P. Bienstman, and D. V. Thourhout, " Nanophotonic waveguide in silicon-on-insulator fabricated with CMOS technology," *J Lightwave Technol*, vol. 23, pp. 401-412, 2005.

[50] R. Soref and J. Lorenzo, "Single-crystal silicon: a new material for 1.3 and 1.6 µm integrated-optical components," *Electronics Letters*, vol. 21, pp. 953-954, 1985.

[51] P. Dumon, W. Bogaerts, V. Wiaux, J. Wouters, S. Beckx, J. V. Campenhout, D. Taillaert, B. Luyssaert, P. Bienstman, D. V. Thourhout, and R. Baets, "Low loss SOI photonic wires and ring resonators fabricated with deep UV lithography," *Photonics Technology Letters, IEEE*, vol. 16, pp. 1328-1330, May 2004.

[52] A. Bazin, "III-V Semiconductor Nanocavitieson Silicon-On-Insulator Waveguide: Laser Emission, Switching and Optical Memory," Université Paris-Diderot - Paris VII, 2013.

[53] W. Bludau, A. Onton, and W. Heinke, "Temperature dependence of Band-Gap of Silicon," *J Appl Phys*, vol. 45, pp. 1846-1848, 1974.

[54] C. Xiong, W.H.P. Pernice, and H.X. Tang, "Low-Loss, Silicon Integrated, Aluminium nitride Photonic Circuits and their use for Electro-optic signal processing," *Nano Letters*, vol. 12, pp. 3562-3568, 2012.

[55] T.J. Kippenberg, A. Schliesser, and M. Gorodetsky, "Phase noise measurement of external cavity diode lasers and implications for optomechanical sideband cooling of GHz mechanical modes," *New Journal of Physics*, vol. 15, p. 015019, 2011.

[56] C. Xiong, W.H.P. Pernice, X. Sun, C. Schuck, K.Y. Fong, and H.X. Tang, "Aluminum nitride as a new material for chip-scale optomechanics and nonlinear optics," *New Journal of Physics*, vol. 14, p. 095014, Oct 2012.

[57] M. Loncar, T. Doll, J. Vuckovic, and A. Scherer, "Design and fabrication of silicon photonic crystal optical waveguides," *J. Lightwave Technol*.,vol. 79, p. 1402, Dec. 2001.

[58] M. Notomi, A. Shinya, K. Yamada, J. Takahashi, C. Takahashi, and I. Yokohama, "Singlemode transmission within photonic bandgap of width varied single-line-defect photonic crystal waveguides on SOI substrates," *Electron. Lett*., vol. 37, pp. 293-295, 2001.

[59] J. Arentoft, T. Sondergaard, M. Kristensen, A. Boltasseva, M. Thorhauge, and L. Frandsen, "Low-loss silicon-on-insulator photonic crystal waveguides," *Electron. Lett*., vol. 38, pp. 274-275, 2002.

[60] M. Mulot, "Two-Dimensional Photonic Crystals in InP-based materials," Doctoral Thesis, Royal Institute of Technology, Stockholm, Sweden, 2004.

[61] Y. J. Dong, B. Z. Tian, T. J. Kempa, and C. M. Lieber, "Coaxial Group III # Nitride Nanowire Photovoltaics," *Nano Letters*, vol. 9, pp. 2183-2187, 2009.

[62] P. Kung and M. Razeghi, "III-Nitride wide bandgap semiconductors: a survey of the current status and future trends of the material and device technology," *Opto-Electronics Review*, vol. 8, pp. 201-239, 2000.

[63] W.H.P. Pernice, C. Xiong, C. Schuck, and H.X. Tang, "High Q aluminium nitride photonic crystal nanobeam cavities," *Appl Phys Lett*, vol. 100, p. 091105, 2012.

[64] W.H.P. Pernice, C. Xiong, C. Schuck, and H.X. Tang, "High Q micro-ring resonators fabricated from polycrystalline aluminium nitride films for near infrared and visible photonics," *Opt. Express*, vol. 20, pp. 12261-12269, 2012.

[65] C. Xiong, X. K. Sun, K. Y. Fong, and H. X. Tang, "Integrated high frequency aluminium nitride optomechanical resonators," *Appl Phys Lett*, vol. 100, p. 171111, 2012.

[66] K.S.A. Butcher and T. l. Tansley, "InN, latest development and a review of the band-gap controversy," *Superlattices and Microstructures*, vol. 38, pp. 1-37, 2005.

[67] T. Kachi, T. Tomita, K. Itoh, and H. Tadano, "A new buffer layer for high-quality GaN growth by metalorganic vapor-phase epitaxy," *Applied Physics Letters*, vol. 72, pp. 704-706, 1998.

[68] V. Chaudhari, "Growth of Indium Nitride and Gallium Nitride on Silicon using metal organic hydride vapour phase epitaxy," Ph.D. dissertation, University of Florida, Gainesville, United States, 2012.

[69] N. Shahid, "Technology and properties of InP based photonic crystal structure and devices", Ph.D. dissertation, Division of Semiconductor Materials, KTH School of Information and Communication Technology, Stockholm, Sweden, 2012.

[70] D. Meade, A. M. Rappe, K. D. Brommer, and J. D. Joannopoulos, "Existence of a photonic band gap in two dimensions," *Appl. Phys. Lett.*, vol. 61, pp. 495-497, 1992.

thesis file

ORIGINALITY REPORT

16%	4%	14%	2%
SIMILARITY INDEX	INTERNET SOURCES	PUBLICATIONS	STUDENT PAPERS

PRIMARY SOURCES

1	Goyal, Amit Kumar, and Suchandan Pal. "Design and simulation of high-sensitive gas sensor using a ring-shaped photonic crystal waveguide", Physica Scripta, 2015. Publication	3%
2	Zhao, Yong, Ya-Nan Zhang, Qi Wang, and Haifeng Hu. "Review on the Optimization Methods of Slow Light in Photonic Crystal Waveguide", IEEE Transactions on Nanotechnology, 2015. Publication	2%
3	Hamza Kurt. "Annular photonic crystals", Optics Express, 2005 Publication	1%
4	Encyclopedia of Microfluidics and Nanofluidics, 2015. Publication	1%
5	Jamois, C.. "Silicon-based two-dimensional photonic crystal waveguides", Photonics and Nanostructures - Fundamentals and Applications, 200312 Publication	1%